J|A|C|S
ARTICLES
Published on Web 11/27/2003

Ruthenacarboranes from the Reaction of *nido*-1,2-$(Cp^*RuH)_2B_3H_7$ with $HC{\equiv}CCO_2Me$, $Cp^* = \eta^5$-C_5Me_5. Hydrometalation, Alkyne Incorporation, and Functional Group Modification via Cooperative Metal−Boron Interactions within a Metallaborane Cluster Framework

Hong Yan,* Alicia M. Beatty, and Thomas P. Fehlner*

Contribution from the Department of Chemistry and Biochemistry, University of Notre Dame, Notre Dame, Indiana 46556-5670

Received September 10, 2003; E-mail: fehlner.1@nd.edu

Abstract: Reaction of *nido*-1,2-$(Cp^*RuH)_2B_3H_7$, **1**, and methyl acetylene monocarboxylate under kinetic control generates *nido*-1,2-$(Cp^*Ru)_2(\mu$-C{[CO_2Me]Me}$)B_3H_7$ (a pair of geometric isomers, **3** and **5**) and *nido*-1,2-$(Cp^*Ru)_2$(1,3-μ-C{[CH_2CO_2Me]H}$)B_3H_7$, **4**, which display the first examples of exo-cluster μ-alkylidene Ru−B bridges generated by hydrometalation of an alkyne on the cluster framework. Both **3** and **5**, but not **4**, rearrange into *arachno*-2,8-μ(C)-5-η^1(O)-Me{CO_2Me}C-1,2-$(Cp^*Ru)_2B_3H_7$, **2**, in which an unprecedented intramolecular coordination of the carbonyl oxygen atom of the alkyne substituent to a boron framework site opens the ruthenaborane skeleton. Compound **2**, in turn, is an intermediate in the formation of the ruthenacarborane *nido*-1,2-$(Cp^*Ru)_2$-3-OH-4-OMe-5-Me-4,5-$C_2B_2H_5$, **12**, in which the carbonyl−oxygen double bond has been cleaved as its oxygen atom inserts into a B−H bond and the carbonyl carbon inserts into the metallaborane framework. In a parallel reaction pathway, *nido*-1,2-$(Cp^*Ru)_2$-5-CO_2-Me-4,5-$C_2B_2H_7$, **6**, *nido*-1,2-$(Cp^*Ru)_2$-4-$B(OH)_2$-5-CO_2Me-4,5-$C_2B_2H_6$, **16**, and *nido*-1,2-$(Cp^*Ru)_2(\mu$-H$)(\mu$-BH_2)-3-$(CH_2)_2CO_2$Me-CO_2Me-4,5-$C_2B_2H_4$ (a pair of geometric isomers, **7** and **14**, which contain an unusual Ru−B borane bridge) are formed. On heating, **7** rearranges to yield *nido*-1,2-$(Cp^*Ru)_2$-3-$(CH_2)_2CO_2$Me-4-BH_2-5-CO_2Me-4,5-$C_2B_2H_5$, **13**, whereas **14** converts to *nido*-1,2-$(Cp^*Ru)_2$-3-$(CH_2)_2CO_2$Me-4-CO_2Me-4,5-$C_2B_2H_6$, **8**. Under thermodynamic control, *nido*-1,2-$(Cp^*Ru)_2$-4,5-B{$(CH_2)_2CO_2$Me}CO(MeO){$C(CH_2)CO_2$-Me}-4,5-$C_2B_2H_6$, **11**, is the major product accompanied by lesser amounts of **6** and 1,2-$(Cp^*Ru)_2$-4-OMe-5-Me-4,5-$C_2B_2H_6$, **10**. Compound **11** features a five-membered heterocycle containing a boron atom. The structure of **7**, which is an intermediate in the formation of **11**, provides the basis for an explanation of this complex condensation of three alkynes. A previously unrecognized role for an exo-cluster bridging borene generated from the metallaborane skeleton by addition of the alkyne is also a feature of this chemistry. Reinsertion or loss of this boron fragment accounts for much of the chemistry observed. NMR experiments reveal labile intermediates, and one has been sufficiently characterized to provide mechanistic insight on the early stages of the alkyne-metallaborane addition reaction. All isolated compounds have been spectroscopically characterized, and most have been structurally characterized in the solid state.

Introduction

An efficient and high-yield route to dimetallaboranes has been developed on the basis of the reaction of monocyclopentadienylmetal halides (groups 5−9) with monoboranes.[1,2] Such a convenient synthesis of metallaboranes allows their systematic reaction chemistry to be investigated. Selected thermal elimination reactions and addition reactions of metal fragments, monoboranes, and Lewis bases have already been examined.[3−11] The novel chemistry observed clearly demonstrates that the electronic contributions of metal and borane fragments to the cluster structure are expressed in new types of reactivity; that is, the hybrid character of a metallaborane creates reaction possibilities not seen for transition metal complexes or boranes individually.[12−18] Reactions of metallaboranes with alkynes, the focus of this contribution, further verify this statement.

The reactions of transition metal species with alkynes provided early evidence of the wealth of chemistry possible by combining metals and organic moieties.[19,20] Likewise, the

(1) Fehlner, T. P. *J. Chem. Soc., Dalton Trans.* **1998**, 1525.
(2) Fehlner, T. P. *Organometallics* **2000**, *19*, 2643.
(3) Hashimoto, H.; Shang, M.; Fehlner, T. P. *J. Am. Chem. Soc.* **1996**, *118*, 8164.
(4) Lei, X.; Shang, M.; Fehlner, T. P. *J. Am. Chem. Soc.* **1999**, *121*, 1275.
(5) Ghosh, S.; Lei, X.; Cahill, C. L.; Fehlner, T. P. *Angew. Chem., Int. Ed.* **2000**, *39*, 2900.
(6) Macías, R.; Fehlner, T. P.; Beatty, A. M. *Angew. Chem., Int. Ed.* **2002**, *41*, 3860.
(7) Peldo, M. A.; Beatty, A. M.; Fehlner, T. P. *Organometallics* **2002**, *21*, 2821.
(8) DiPasquale, A.; Lei, X.; Fehlner, T. P. *Organometallics* **2001**, *20*, 5044.
(9) Kawano, Y.; Matsumoto, H.; Shimoi, M. *Chem. Lett.* **1999**, 489.
(10) Pangan, L. N.; Kawano, Y.; Shimoi, M. *Organometallics* **2000**, *19*, 5575.
(11) Pangan, L. N.; Kawano, Y.; Shimoi, M. *Inorg. Chem.* **2001**, *40*, 1985.
(12) Grimes, R. N. *Acc. Chem. Res.* **1978**, *11*, 420.

10.1021/ja038444t CCC: $25.00

Scheme 1

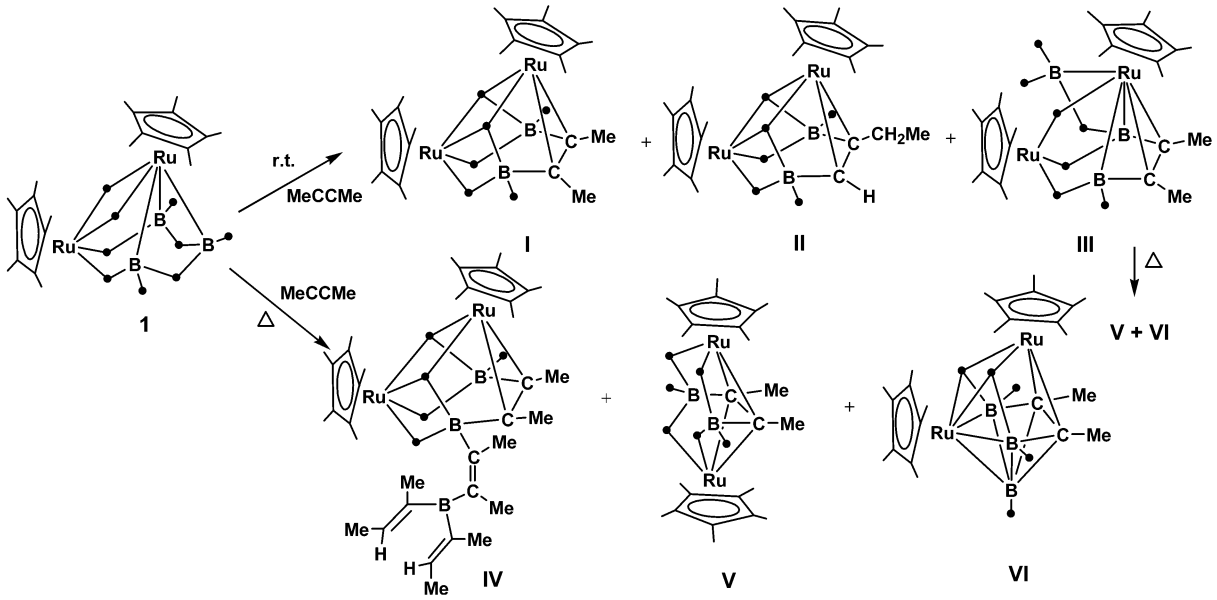

reactions of alkynes with boranes gave rise to hydrocarbyl substituted boranes[21,22] as well as carboranes.[23,24] Many of the latter function as cyclopentadienyl ligand surrogates and fostered a large metallacarborane chemistry.[25−27] Metallaboranes provide a chemical platform to explore metal versus borane site competition for an alkyne, and they constitute an alternative route to metallacarboranes. Indeed, this was recognized 30 years ago by Grimes and co-workers in the generation of the known *nido*-1-CpCo$C_2B_3H_7$,[28] Cp = η^5-C_5H_5, from *nido*-2-CpCo-B_4H_8.[29,30] Some notable contributions followed,[31−33] but development has been slow. This can be attributed to the lack of readily available metallaboranes and little evidence that new metallacarborane types were accessible via this nontraditional route.

The situation changed when metallaboranes did become available and, moreover, when metal type could be selected to provide reactivity under mild conditions where kinetics is expected to determine product distribution. Thus, we have already reported that a hydrogen-rich *nido*-ruthenaborane undergoes alkyne insertion to yield ruthenacarboranes of previously unknown types, some of which can then be converted to more stable compounds (Scheme 1).[34−37] Choice of metal is critical as an isoelectronic dirhodaborane leads predominantly to catalytic cyclotrimerization.[38] To go beyond a rudimentary example of reaction type, a variety of alkynes were investigated. Thus, it was found that terminal alkynes show more diverse chemistries than internal alkynes. This led to consideration of the possibilities presented by a terminal alkyne which also contains a potentially reactive functional group. Here, we describe the rather amazing reaction chemistry of *nido*-1,2-$(Cp^*RuH)_2B_3H_7$, **1**, with the functionalized alkyne HC≡CCO_2Me. Some of these results have been communicated.[36]

Results and Discussion

The reaction of *nido*-1,2-$(Cp^*Ru)_2B_3H_9$, **1**, Cp* = η^5-C_5Me_5, with HC≡CCO_2Me was carried out under three distinctly different conditions. To develop a picture of this complex reaction system, these three regimes are discussed sequentially. First, products isolated by chromatography after reaction under mild conditions are characterized by product structures. Stepwise interconversions verified by NMR analysis permit these compounds to be associated with three distinct reaction manifolds which are treated in the first section following. Second, products formed under more forcing conditions, again isolated as pure compounds and structurally characterized, are described and connected to those formed under mild conditions. Finally, NMR experiments are used to obtain information on species formed under mild conditions on a time scale of minutes rather than hours. These data are used to provide mechanistic information on unstable intermediates connecting the reactants to the isolated products.

(13) Grimes, R. N. In *Metal Interactions with Boron Clusters*; Grimes, R. N., Ed.; Plenum: New York, 1982; p 269.
(14) Kennedy, J. D. *Prog. Inorg. Chem.* **1984**, *32*, 519.
(15) Kennedy, J. D. *Prog. Inorg. Chem.* **1986**, *34*, 211.
(16) Housecroft, C. E. *Boranes and Metalloboranes*; Ellis Horwood: Chichester, 1990.
(17) Smith, M. R., III. *Prog. Inorg. Chem.* **1999**, *48*, 505.
(18) Jan, D.-Y.; Workman, D. P.; Hsu, L.-Y.; Krause, J. A.; Shore, S. G. *Inorg. Chem.* **1992**, *31*, 5123.
(19) Coates, G. E.; Green, M. L. H.; Wade, K. *Organometallic Compounds*, 3rd ed.; Methuen: London, 1967.
(20) Elschenbroich, C.; Salzer, A. *Organometallics*; VCH: New York, 1989.
(21) Wilczynski, R.; Sneddon, L. G. *Inorg. Chem.* **1981**, *20*, 3955.
(22) Wilczynski, R.; Sneddon, L. G. *Inorg. Chem.* **1982**, *21*, 506.
(23) Muetterties, E. L., Ed. *Boron Hydride Chemistry*; Academic Press: New York, 1975.
(24) Grimes, R. N. *Carboranes*; Academic Press: New York, 1970.
(25) Hawthorne, M. F.; Dunks, G. B. *Science* **1972**, *178*, 462.
(26) Hawthorne, M. F. *J. Organomet. Chem.* **1975**, *100*, 97.
(27) Grimes, R. N. *Coord. Chem. Rev.* **1979**, *28*, 47.
(28) Grimes, R. N.; Beer, D. C.; Sneddon, L. G.; Miller, V. R.; Weiss, R. *Inorg. Chem.* **1974**, *13*, 1138.
(29) Grimes, R. N. *Pure Appl. Chem.* **1974**, *39*, 455.
(30) Weiss, R.; Bowser, J. R.; Grimes, R. N. *Inorg. Chem.* **1978**, *17*, 1522.
(31) Ditzel, E. J.; Fontaine, X. L. R.; Greenwood, N. N.; Kennedy, J. D.; Sisan, Z.; Stibr, B.; Thornton-Pett, M. *J. Chem. Soc., Chem. Commun.* **1990**, 1741.
(32) Bould, J.; Rath, N. P.; Barton, L.; Kennedy, J. D. *Organometallics* **1998**, *17*, 902.
(33) Bould, J.; Rath, N. P.; Barton, L. *Organometallics* **1996**, *15*, 4916.
(34) Yan, H.; Beatty, A. M.; Fehlner, T. P. *Angew. Chem., Int. Ed.* **2001**, *40*, 4498.
(35) Yan, H.; Beatty, A. M.; Fehlner, T. P. *Angew. Chem., Int. Ed.* **2002**, *41*, 2578.
(36) Yan, H.; Beatty, A. M.; Fehlner, T. P. *J. Am. Chem. Soc.* **2002**, *124*, 10280.
(37) Yan, H.; Beatty, A. M.; Fehlner, T. P. *J. Organomet. Chem.* **2003**, *680*, 66.
(38) Yan, H.; Beatty, A. M.; Fehlner, T. P. *Organometallics* **2002**, *21*, 5029.

Scheme 2

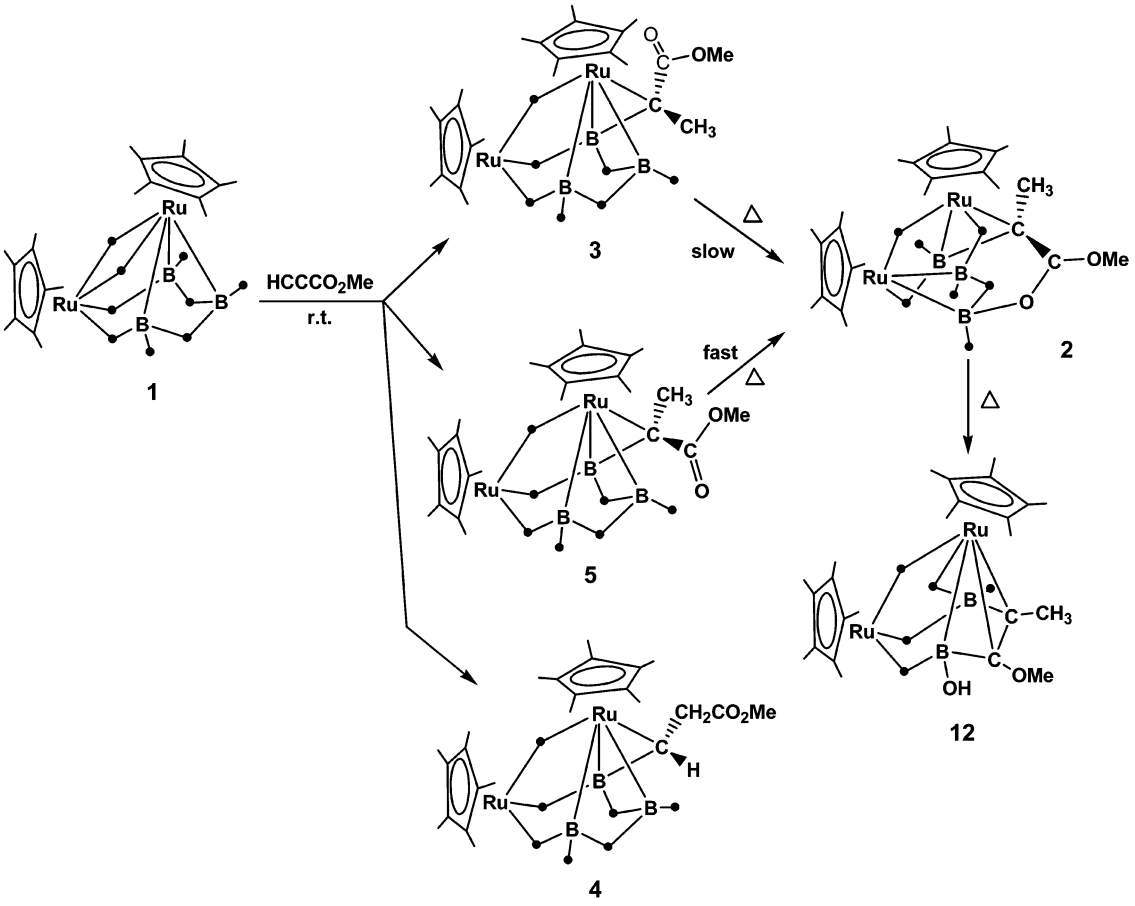

Scheme 3 [a]

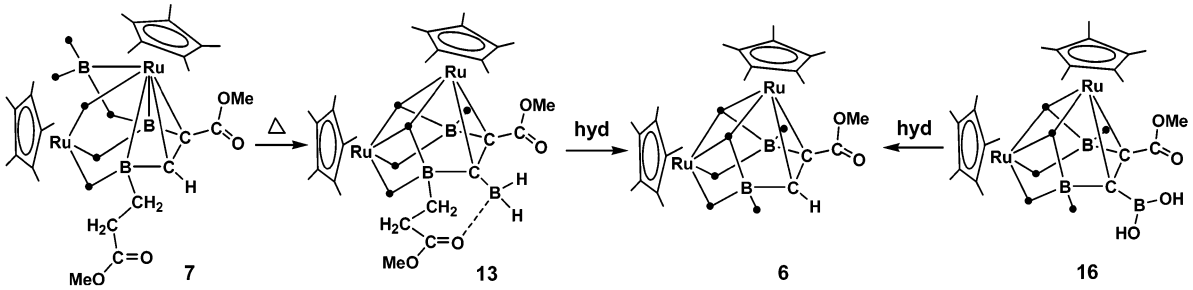

[a] (hyd = hydrolysis).

Scheme 4

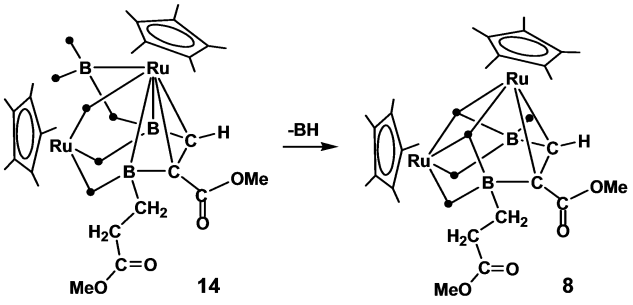

Kinetically Controlled Regime. The versatile reactivity of a *nido*-diruthenapentaborane is summarized in the three reaction sequences shown in Schemes 2−4 and is discussed in the following section.

The Conversion of *nido*-1,2-(Cp*Ru)$_2$B$_3$H$_9$, 1, into 1,2-(Cp*Ru)$_2$-3-OH-4-OMe-5-Me-4,5-C$_2$B$_2$H$_5$, 12. Reaction of **1** with methyl acetylene monocarboxylate at ambient temperature produces *nido*-1,2-(Cp*Ru)$_2$(1,3-μ-C{[CO$_2$Me]Me})B$_3$H$_7$, **3** and **5**, and *nido*-1,2-(Cp*Ru)$_2$(1,3-μ-C {[CH$_2$CO$_2$Me]H})B$_3$H$_7$, **4**, isolated in yields of 10%, 10%, and 4%, respectively (Scheme 2). The X-ray structures, shown in Figures 1−3, display the ruthenaborane framework of **1** appended with a novel μ-alkylidene Ru−B bridge derived from hydrogenation of the alkyne by two cluster hydrogen atoms. Compounds **3** and **5** are geometrical isomers differing in the orientation of the Me and CO$_2$Me groups relative to the Ru−Ru edge of the cluster. In **3**, the methyl ester group refines in two positions in the solid state, which are related by the exchange of the carbonyl oxygen and the OMe group (Figure 1a and b). In solution, however, only a single resonance for the CH$_3$ group appears in the ^{1}H and ^{13}C

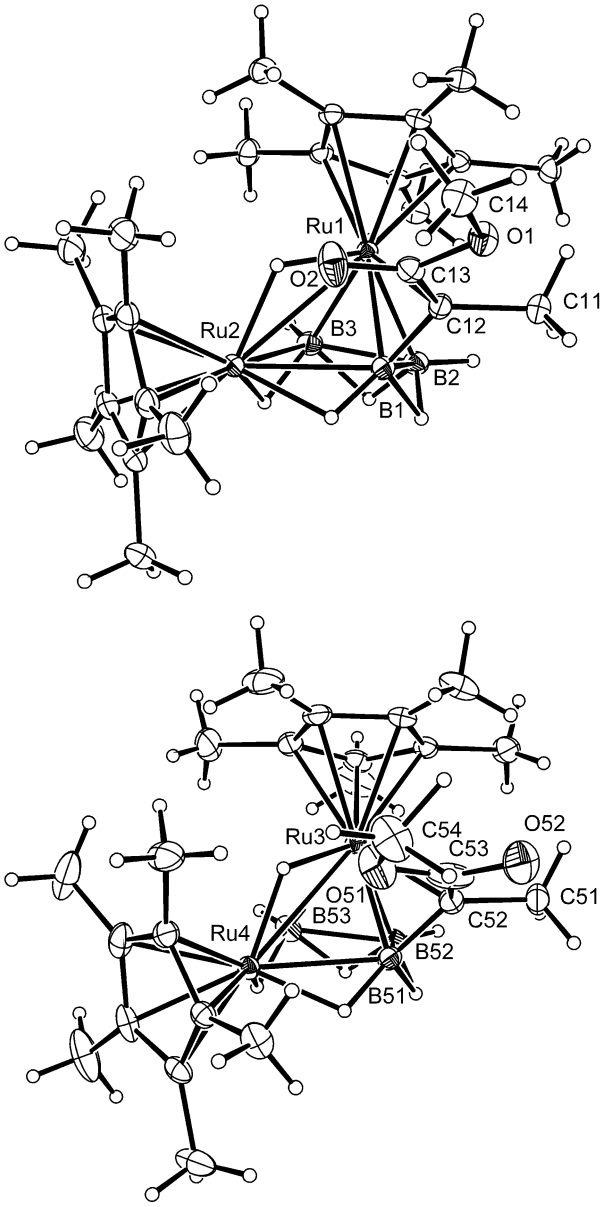

Figure 1. Molecular structure of **3** showing the two rotameric forms refined as a nearly 1:1 mixture. Selected bond lengths (Å): Ru(1)−Ru(2) 2.8806(2), Ru(1)−B(1) 2.1060(19), Ru(1)−B(2) 2.1351(19), Ru(1)−B(3) 2.1643(19), Ru(1)−C(12) 2.2655(17), Ru(2)−B(1) 2.3631(19), Ru(2)−B(3) 2.331(2), B(1)−B(2) 1.860(3), B(2)−B(3) 1.824(3), O(1)−C(13) 1.362(2), O(1)−C(14) 1.435(2), O(2)−C(13) 1.211(2), B(1)−C(12) 1.519(3), C(11)−C(12) 1.520(2), C(12)−C(13) 1.482(2).

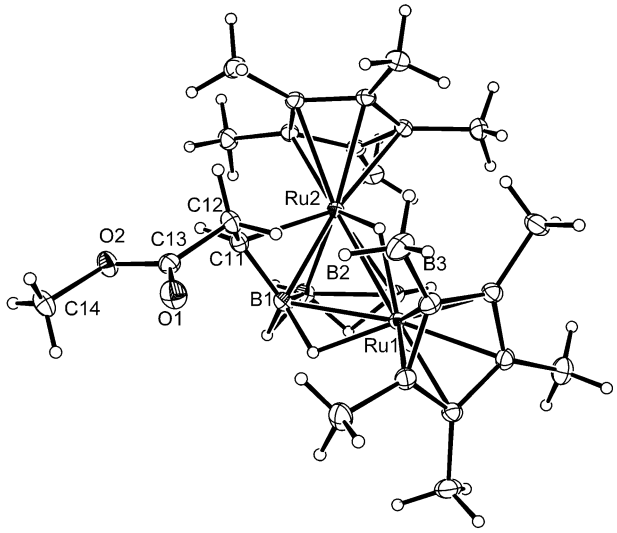

Figure 2. Molecular structure of **4**. Selected bond lengths (Å): Ru(1)−B(1) 2.3886(16), Ru(1)−B(3) 2.3319(17), Ru(1)−Ru(2) 2.87420(18), Ru(2)−B(1) 2.1368(16), Ru(2)−B(2) 2.1264(17), Ru(2)−B(3) 2.1772(17), B(1)−B(2) 1.840(2), B(2)−B(3) 1.830(2), B(1)−C(11) 1.499(2), O(1)−C(13) 1.2106(19), O(2)−C(13) 1.3477(18), O(2)−C(14) 1.4453(18), C(11)−C(12) 1.522(2), C(12)−C(13) 1.508(2).

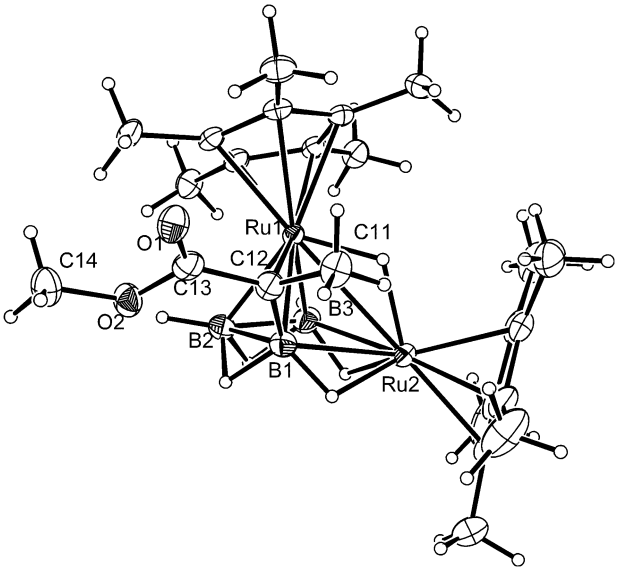

Figure 3. Molecular structure of **5**. Selected bond lengths (Å): Ru(1)−B(1) 2.119(4), Ru(1)−B(2) 2.132(4), Ru(1)−B(3) 2.174(4), Ru(1)−Ru(2) 2.8816(4), Ru(1)−C(12) 2.261(3), Ru(2)−B(1) 2.368(4), Ru(2)−B(3) 2.321(4), B(1)−B(2) 1.823(5), B(2)−B(3) 1.825(5), B(1)−C(12) 1.511(5), O(1)−C(13) 1.207(4), O(2)−C(13) 1.361(5), O(2)−C(14) 1.437(4), C(11)−C(12) 1.519(5), C(12)−C(13) 1.478(5).

spectra. Both **3** and **5** are chiral (racemic mixture resulting from bridging the two equivalent Ru−B edges of **1** in equal numbers) and result from putative dihydrometalation on the external surface of the cluster with Markovnikov regiochemistry. The barrier to interconversion of the isomers is larger than that for conversion to a more stable product (see below), and the most stable isomer could not be indentified.

Compound **4** is a valence isomer of **3** and **5** with regiochemistry that reflects anti-Markovnikov addition of H. The presence of a $CHCH_2CO_2Me$ fragment with a diastereotopic methylene group is confirmed by the ^1H spectrum, which exhibits three aliphatic C−H protons of appropriate multiplicities (a broad doublet, $J = 4.4$ Hz, a doublet of doublets, $J_1 = 4.4$ Hz, $J_2 = 14$ Hz, and a doublet of doublets, $J_1 \approx J_2 = 14$ Hz), and the ^{13}C spectrum (broad B−CH at 57.36 ppm and sharp aliphatic CH_2 at 43.43 ppm). The orientation of the CO_2Me group relative to the cluster framework resembles that of **5**: the isomer corresponding to **3** was not found. A structurally characterized analogue of **4** from the reaction of **1** with HC≡CPh has been described; however, no Markovnikov products at all were isolated with this alkyne.[37] Compounds containing metal−boron μ-alkylidenes were unknown previous to this work, although M−M bridging CR_2 fragments are well known in transition metal organometallic chemistry.[20]

All three compounds possess structures in which the alkyne has been converted into a μ-alkylidene by addition of two cluster hydrogen atoms of **1**. As the bridging alkylidene is a two electron contributor to cluster bonding, the skeletal electron pair

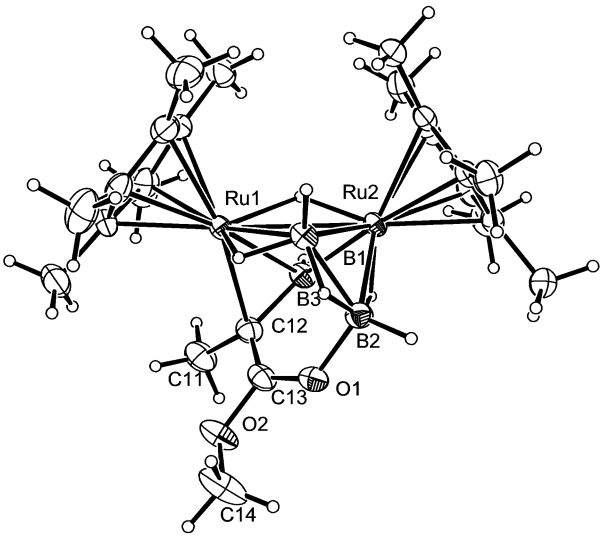

Figure 4. Molecular structure of **2**. Selected bond lengths (Å): Ru(1)−C(12) 2.275(3), Ru(1)−B(1) 2.301(3), Ru(1)−B(3) 2.335(3), Ru(1)−Ru(2) 2.9184(3), Ru(2)−B(1) 2.175(3), Ru(2)−B(2) 2.178(3), Ru(2)−B(3) 2.229(3), O(1)−C(13) 1.292(3), O(1)−B(2) 1.504(4), B(1)−B(2) 1.788(4), O(2)−C(13) 1.342(3), O(2)−C(14) 1.441(4), B(3)−C(12) 1.540(4), C(11)−C(12) 1.531(4), C(12)−C(13) 1.399(4).

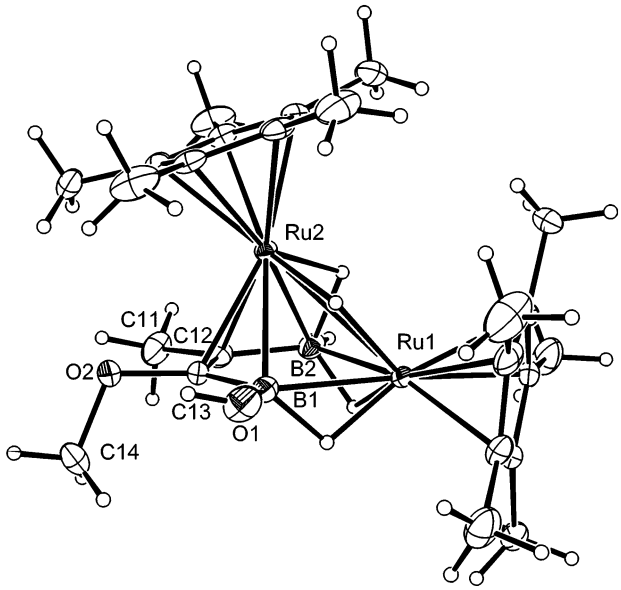

Figure 5. Molecular structure of **12**. Selected bond lengths (Å): Ru(1)−B(1) 2.301(2), Ru(1)−B(2) 2.458(2), Ru(1)−Ru(2) 2.9471(2), Ru(2)−B(1) 2.480(2), Ru(2)−B(2) 2.327(2), Ru(2)−C(12) 2.2095(17), Ru(2)−C(13) 2.2154(18), B(1)−O(1) 1.396(3), B(1)−C(13) 1.535(3), B(2)−C(12) 1.548(3), C(11)−C(12) 1.513(3), C(12)−C(13) 1.408(3), O(2)−C(13) 1.424(2), O(2)−C(14) 1.427(3).

(sep) count remains the same and the *nido* square pyramidal geometry of **1** is retained. Stoichiometrically, these two hydrogen atoms arise from one B−Ht terminal hydrogen and one bridging Ru−H−Ru hydride. If the mechanism follows stoichiometry, generation of CH_3 in **3** and **5** and CH_2 in **4** arises from hydroboration and hydroruthenation. This would be difficult to prove as rearrangement of hydrogen atoms on a cluster framework can be very fast,[39−42] and the actual origin is unknown. Simplicity does argue for intramolecular hydrometalation after coordination of the alkyne.

Controlled thermolysis of either **3** or **5** generates *arachno*-2,8-μ(C)-5-η^1(O)-Me{CO_2Me}C-1,2-(Cp*Ru)$_2B_3H_7$, **2**. The structure determination (Figure 4) reveals an unusual structure. The spectroscopic data support the placement of the endo-hydrogen atoms on the framework as shown in Scheme 2. The $^1H\{^{11}B\}$ spectrum exhibits an apparent quartet ($J \approx 10$ Hz) for the B−H−B proton resonance consistent with coupling to the adjacent two B−Ht (d, $J \approx 10$ Hz) protons and bridging B−H−Ru (d, $J \approx 10$ Hz) proton. The other bridging B−H−Ru proton and its adjacent B−Ht proton show no measurable coupling and appear as singlets in the $^1H\{^{11}B\}$ spectrum. Hence, reflecting the contorted nature of its framework, **2** exhibits bridging B−H−Ru to both Ru centers which, in turn, are bridged by a Ru−H−Ru hydrogen.

Although unusual, the structure of **2** easily follows from the structure of **5**. In forming **2**, the carbonyl oxygen of the bridging alkylidene coordinates to the unique boron atom of **5** and opens one B−H−B edge of the *nido* framework. The B−O distance (1.50 Å) is close to the sum of the covalent radii albeit longer than a typical B−O distance.[43] The pair of electrons contributed by the oxygen atom to the cluster bonding network increases the sep to 8, thereby generating the observed open *arachno* structure of the Ru_2B_3 cluster core. A measure of the strength of internal coordination is also evident in most of the structural parameters. As compared to **5**, the C−O distance increases ∼0.1 Å and ν(C−O) decreases ∼200 cm^{-1}, whereas the chemical shift of its ^{13}C resonance (183 ppm) changes little (179 ppm in **5**).

The conversion of **5** to **2** is much more facile ($t_{1/2} = 10$ min at 80 °C) than that of **3** to **2** ($t_{1/2} = 8$ h at 80 °C); that is, the reaction barrier for **3** is larger than that for **5**. Monitoring the conversion of **3** into **2** by ^1H NMR did not reveal **5** as an intermediate. Hence, if the conversion of **3** proceeds via **5**, the conversion of **5** to **2** must be more rapid than the generation of **5** from **3**. Note that in **3** the methyl ester group is positioned over the metals whereas in **5** the carbonyl oxygen is perfectly positioned to attack the BH fragment in the 4-position, which is the one coordinated by the oxygen atom in **2** (Scheme 2). Hence, a consecutive mechanism, in which the rearrangement of **3** to **5** is the rate-determining step, is a logical one. Heating of **4**, which has the geometry of **3**, at 80 °C for 24 h leads to decomposition. Either the isomer corresponding to **5** is not accessible or the geometric requirements of the intramolecular reaction producing an analogue of **2** are not met.

Further heating **2** generates **12** which is a pentagonal pyramidal 8 sep *nido* ruthenacarbahexaborane similar to that found for unfunctionalized alkynes (**I**, Scheme 1). The spectroscopic data in solution are consistent with the solid-state structure (Figure 5) and confirm H locations. The ^1H spectrum shows one Ru−H−Ru hydride, three B−H−Ru hydrogens, and one B−OH proton (broad signal at 2.3 ppm). The $^1H\{^{11}B\}$ spectrum reveals that two of the B−H−Ru resonances are doublets with coupling constants reflecting coupling with the respective B−Ht. The other B−H−Ru resonance is a singlet and is assigned to that adjacent to the B−OH fragment. The IR spectrum now shows a OH stretch at 3588 cm^{-1} but no C═O stretch similar to that of **2**. The ^{13}C spectrum shows no C═O

(39) Getman, T. D.; Krause, J. A.; Shore, S. G. *Inorg. Chem.* **1988**, *27*, 2398.
(40) Deeming, A. J.; Underhill, M. *J. Chem. Soc., Chem. Commun.* **1973**, 277.
(41) Evans, J.; Street, A. C.; Webster, M. *Organometallics* **1987**, *6*, 794.
(42) Ohki, Y.; Uehara, N.; Suzuki, H. *Organometallics* **2003**, *22*, 59.
(43) Greenwood, N. N.; Earnshaw, A. *Chemistry of the Elements*; Pergamon Press: Oxford, 1984.

resonance but now contains two broad carbon resonances (95.5 and 100.3 ppm) characteristic of the two framework carbon atoms.

In the reaction that coverts **2** to **12**, the C−O bond of the boron activated carbonyl group has been cleaved and the O atom inserted into the B−H bond of the boron atom to which it was coordinated. Concomitant with BOH formation, the carbonyl carbon atom and the adjacent carbyne carbon are incorporated into the metallaborane framework with overall loss of a [BH] fragment. The ultimate fate of the [BH] fragment is unknown, but BH vertex loss from borane skeletons is well precedented.[44−46] The final product has the stable 8 sep pentagonal pyramidal core structure similar to that observed earlier for internal alkynes.[34]

The overall reaction sequence, from **1** to **3**, **5** to **2**, and then to **12**, demonstrates reduction of a ≡CH fragment to CH_3, insertion of carbonyl oxygen into a B−H bond, and insertion of a C_2 fragment into a ruthenaborane cluster. Individually, all of the processes are known. For example, the reaction of $\{Cp^*Ru(\mu\text{-}H)\}_3(\mu_3\text{-}H)_2$ with acetylene generates a M−M μ-ethylidene complex $\{Cp^*Ru(\mu\text{-}H)\}_3(\mu\text{-}CMeH)\{(\mu_3\text{-}\eta^2\text{-}(CH{=}CH)\}$;[47] the insertion of CO into the BH bond in the reaction of CO with B_2H_6 catalyzed by BH_4^- yields methyl boroxine;[48,49] and the insertion of acetylene into *nido*-2-$CpCoB_4H_8$ produces *nido*-1-$CpCoC_2B_3H_7$.[29] Yet what is impressive about this system is that all three take place sequentially on a single metallaborane framework and reflect the multipurpose nature of a metallaborane. Consistent with earlier metallaborane reaction chemistry,[50] the cluster framework is not simply an inert support but an active participant in the reaction. Indeed, cluster "breathing" mechanisms, in which the cluster opens and closes during the course of intermolecular addition of a Lewis base, have been established earlier for both metal and borane cluster systems.[51,52] This work has produced the first example of the intramolecular analogue.

Two Routes Leading to *nido*-1,2-$(Cp^*Ru)_2$-5-CO_2Me-4,5-$C_2B_2H_7$, 6. A diruthena-dicarba-diborane cluster, formed by incorporation of the alkyne into the borane framework of **1** with loss of the elements [BH_3], is a stable product of reaction with internal alkynes (**I**, Scheme 1).[37] Hence, the analogous derivative, **6**, was an expected product. In contrast to **3**−**5**, **6** is isolated under all reaction conditions explored with a yield that depends on reaction conditions as well as isolation procedures. As **6** can be generated during chromatography of certain products (see below), it is important to note that it was observed by NMR in the product reaction mixture.

A solid-state structure determination shows that **6**, like **12**, possesses an 8 sep *nido* $Ru_2B_2C_2$ framework containing two boron atoms and one inserted alkyne (Figure 6). The spectroscopic data are consistent with this conclusion, albeit one carbyne carbon ^{13}C resonance was not observed. The signature of the ^1H resonances of the endo-cluster hydrogens is characteristic of the $M_2B_2C_2$ *nido* skeleton, and, as it permits the assignment of several compounds discussed below that lack structure determinations, we present pertinent details. Of the four high field resonances for M−B endo-hydrogen atoms, two are broad and easily assigned to B−H−Ru bridges. The other two are less broad but not as sharp as those of typical Ru−H−Ru hydrides. A 1D $^1H\{^{11}B\}$ spectrum shows each of the Ru−H−Ru protons is coupled to its adjacent B−H−Ru and B−Ht protons and are observed as apparent triplets (dd with J's $\approx$ 7 Hz). The B−H−Ru protons and the B−Ht protons are also apparent triplets. The only reasonable assignment is hydrogen atoms triply bridging the Ru_2B faces. Corroboration comes from the solid-state structure determination where residual electron density is found approximately centered on the Ru_2B triangular faces.

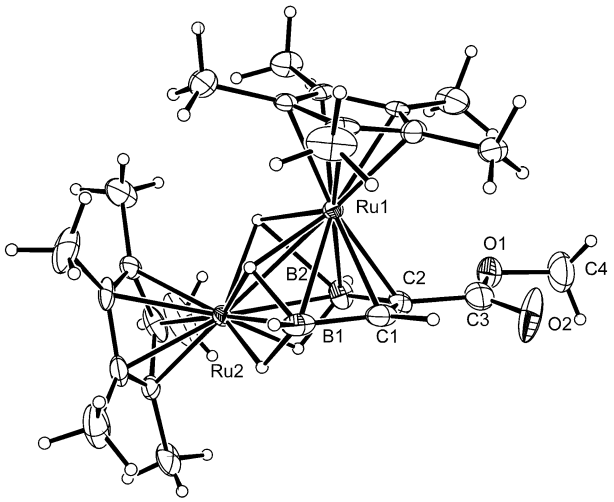

Figure 6. Molecular structure of **6**. Selected bond lengths (Å): Ru(1)−C(1) 2.170(8), Ru(1)−C(2) 2.180(8), Ru(1)−B(1) 2.358(10), Ru(1)−B(2) 2.360(10), Ru(1)−Ru(2) 2.9424(10), Ru(2)−B(1) 2.399(10), Ru(2)−B(2) 2.385(10), O(1)−C(3) 1.352(11), O(1)−C(4) 1.448(11), O(2)−C(3) 1.208(11), B(1)−C(1) 1.508(14), B(2)−C(2) 1.557(13), C(1)−C(2) 1.391(12), C(2)−C(3) 1.493(12).

Why should **6** differ from **1** in this regard? One possibility is that the basal borane fragments do not compete effectively with the framework C_2 moiety for the apical Ru atom and are forced to interact with the Ru−H−Ru bridges. Note that the C−C distance is 1.39 Å, which is similar to that found in *nido*-$C_2B_4H_8$.[23] With equal numbers of B, Ru, and C atoms in the framework, **6** may well express the hybrid character of a compound lying between that of a metallacarborane cluster and an organometallic complex containing a putative organoborane ligand. Consistent with this explanation is the observation that the behavior of the metal hydrides of **12** lies between that of **1** and **6**; that is, the electron-rich BOH fragment competes with CR but the BH does not, thereby generating the unusual hydride arrangement observed (Scheme 2).

Highly polar *nido*-1,2-$(Cp^*Ru)_2$-4-$B(OH)_2$-5-CO_2Me-4,5-$C_2B_2H_6$, **16**, was isolated (7%) and is one progenitor of **6** on workup. A structure determination (Figure 7) reveals an 8 sep *nido* $Ru_2B_2C_2$ cluster with two triply bridging hydrides similar to those of **6**. Curiously, the inserted alkyne now bears a $B(OH)_2$ substituent which is confirmed by the IR, ^{11}B, and ^1H NMR spectra. Pure **16** was obtained by repeated column chromatography because it is mixed with several species of similar high polarity. On chromatography of **16**, **6** is generated and a

(44) Morrey, J. R.; Johnson, A. B.; Fu, Y.-C.; Hill, G. R. *Adv. Chem. Ser.* **1961**, *32*, 157.
(45) Venable, T. L.; Grimes, R. N. *Inorg. Chem.* **1982**, *21*, 887.
(46) Goodreau, B. R.; Orlando, L. R.; Spencer, J. T. *J. Am. Chem. Soc.* **1992**, *114*, 3827.
(47) Takao, T.; Takemori, T.; Moriya, M.; Suzuki, H. *Organometallics* **2002**, *21*, 5190.
(48) Rathke, M. W.; Brown, H. C. *J. Am. Chem. Soc.* **1966**, *88*, 2606.
(49) Onak, T. *Organoborane Chemistry*; Academic Press: New York, 1975.
(50) Ghosh, S.; Lei, X.; Shang, M.; Fehlner, T. P. *Inorg. Chem.* **2000**, *39*, 5373.
(51) Shriver, D. F., Kaesz, H. D., Adams, R. D., Eds. *The Chemistry of Metal Cluster Complexes*; VCH: New York, 1990.
(52) Gaines, D. F. *Acc. Chem. Res.* **1973**, *6*, 416.

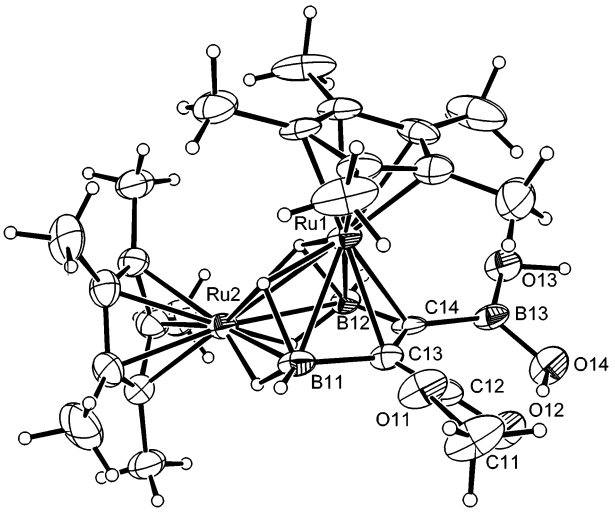

Figure 7. Molecular structure of **16**. Selected bond lengths (Å): Ru(1)−C(13) 2.166(5), Ru(1)−C(14) 2.201(4), Ru(1)−B(11) 2.339(6), Ru(1)−B(12) 2.365(5), Ru(1)−Ru(2) 2.9461(6), Ru(2)−B(11) 2.332(6), Ru(2)−B(12) 2.370(6), B(11)−C(13) 1.563(8), B(12)−C(14) 1.549(8), C(12)−C(13) 1.479(7), B(13)−O(14) 1.360(7), B(13)−O(13) 1.372(7), B(13)−C(14) 1.573(8), C(13)−C(14) 1.433(7).

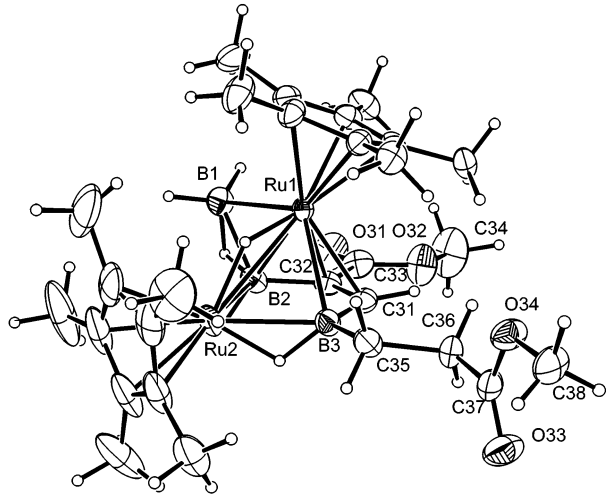

Figure 8. Molecular structure of **7**. Selected bond lengths (Å): Ru(1)−B(2) 2.166(3), Ru(1)−C(32) 2.175(3), Ru(1)−C(31) 2.225(3), Ru(1)−B(1) 2.304(3), Ru(1)−B(3) 2.465(3), Ru(1)−Ru(2) 2.9335(3), B(1)−B(2) 1.776(5), Ru(2)−B(2) 2.296(3), Ru(2)−B(3) 22.304(3), B(2)−C(32) 1.532(5), B(3)−C(31) 1.522(5), B(3)−C(35) 1.603(5), C(31)−C(32) 1.420(4), C(32)−C(33) 1.480(5), C(35)−C(36) 1.586(6).

prolonged chromatographic procedure results in complete decomposition of **16** to **6**. Attempts to trace the origin of **16** in earlier species resulted in the isolation of two intermediates containing fully reduced alkynes. All attempts at crystallization led to crystals of **16**, and the spectroscopic data for these labile intermediates were not sufficient to define their structures. However, these results show that hydrocarbyl substituents on boron can be lost: a point reinforced in the chemistry that follows.

nido-1,2-$(Cp^*Ru)_2(\mu\text{-}H)(\mu\text{-}BH_2)$-3-$(CH_2)_2CO_2Me$-5-$CO_2Me$-4,5-$C_2B_2H_4$, **7**, was isolated (9%), and its solid-state structure (Figure 8) shows the now familiar 8 sep $Ru_2B_2C_2$ core framework found in **6** but one that bears an exo-cluster bridging BH_2 unit plus a terminal hydrocarbyl substituent on one boron atom. The former structural feature was observed with internal alkynes (**III** in Scheme 1), and the discussion of its unique

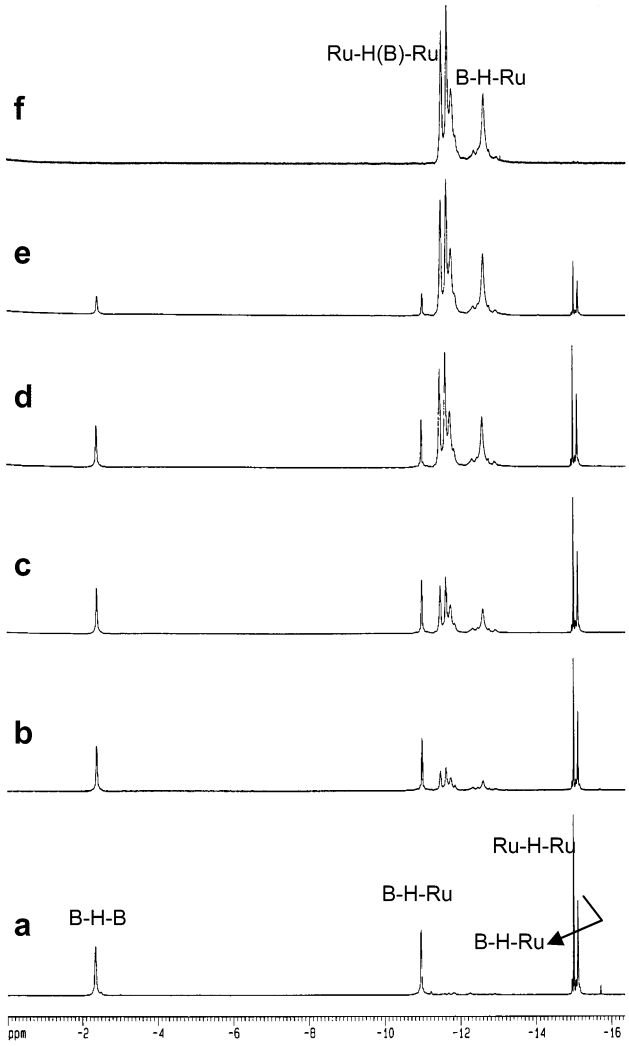

Figure 9. $^1H\{^{11}B\}$ NMR monitoring the conversion of **7** to **13** in the high field in C_6D_6. (a) **7** at room temperature; (b) 10 min at 65 °C; (c) 30 min at 65 °C; (d) 50 min at 65 °C; (e) 1.5 h at 65 °C; (f) 1 h at 80 °C (**7** is completely converted to **13**).

characteristics will not be repeated here.[37] Formation of **7** requires two alkynes; that is, one inserts into the framework and the other is fully hydrometalated to become the saturated hydrocarbon substituent on a framework B atom. Generation of the latter from a bridging alkylidene exemplified by **4** is an attractive possibility. Once again, the spectroscopic data are fully consistent with the solid-state structure. Two sets of aliphatic CH_2 resonances (complex multiplets) in the ^1H NMR as well as one sharp and one broad CH_2 in the ^{13}C spectrum are characteristic of the presence of the reduced alkyne substituent. An analogue of **7** was also isolated from the reaction of **1** with HC≡CPh.[37] It contains an exopolyhedral BH_2 as well as one fully reduced alkyne, albeit with the phenyl group rather than the C−H hydrogen atom adjacent to the hydrocarbyl substituent.

Because the known analogues of **7** are intermediates in the formation of subsequent products,[35] the presence of an exo-BH_2 unit on **7** suggests similar behavior is probable. Indeed, *nido*-1,2-$(Cp^*Ru)_2$-3-$(CH_2)_2CO_2Me$-4-BH_2-5-CO_2Me-4,5-$C_2B_2H_5$, **13**, is formed exclusively when **7** is heated (Figures 9 and 10). As suitable crystals were not obtained, the composition and structure of **13** is based on spectroscopic data. Precise mass measurements on one component of the parent ion envelope

Table 1. ^{13}C Chemical Shifts (in C_6D_6) for Framework Carbon Atoms

	7	13	8	11	I[a]	II[a]	III[a]	IV[a]	V[a]
C−B	95.0 (B−CH)	93.3	97.5 (B−CH)	101.1	108.5	97.5 (B−CH)	115.5	101.5	87.8
C−B	97.9	148.3 (B−C−B)	93.9	134.0 (B−C−B)	108.5	118.8	128.4	109.8	87.8
other C−B								145.5 145.8 152.4	

[a] See Scheme 1.

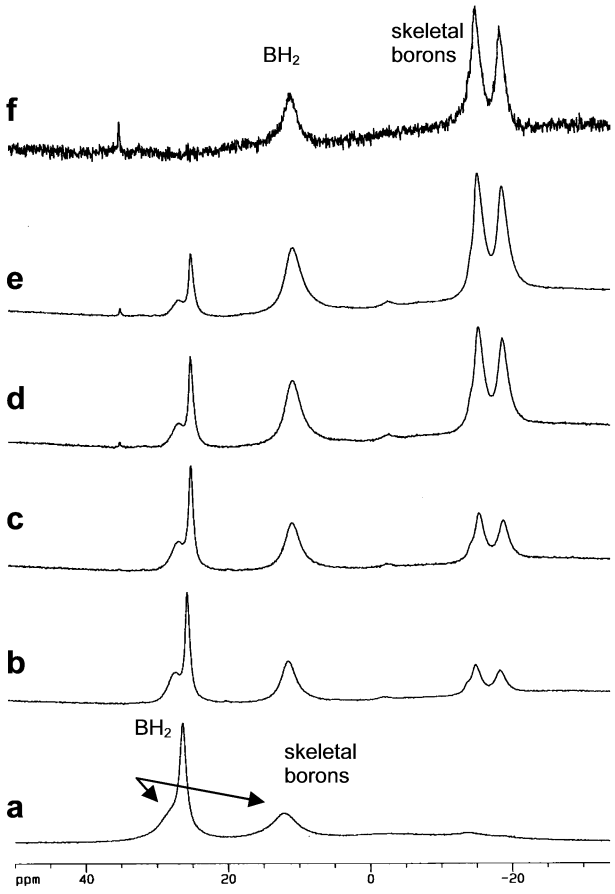

Figure 10. $^{11}B\{^1H\}$ NMR monitoring the conversion of **7** to **13** in C_6D_6. (a) **7** at room temperature; (b) 10 min at 65 °C; (c) 30 min at 65 °C; (d) 50 min at 65 °C; (e) 1.5 h at 65 °C; (f) 1 h at 80 °C (**7** is completely converted to **13**).

yield a composition of $C_{28}H_{44}O_4B_3Ru_2$, showing that a rearrangement has taken place without loss of any atoms except possibly hydrogen. The ^1H spectrum confirms the presence of two Cp*, two OMe, two aliphatic CH_2 (multiplets), two B−Ht in a ratio of 1: 2, two Ru_2B face-bridging, and two B−H−Ru edge-bridging hydrogen atoms. The loss of the characteristic signature of the exopolyhedral BH_2 fragment of **7** suggests a rearrangement involving this fragment has taken place. The line widths of the three signals in the $^{11}B\{^1H\}$ spectrum obscure splitting from B−H coupling; however, comparison of peak widths in coupled and decoupled spectra is consistent with one B−R and two B−H_x fragments. As three B−Ht protons are observed, the molecule contains BH and a BH_2 group. The latter is assigned to the broadest coupled resonance.

Earlier we found that an exo-BH_2 unit may reinsert into a cluster to form a *closo* structure.[35] What is the fate of the exo-BH_2 in the case of **7**? The ^{13}C spectrum is informative. In addition to two Cp*, two CO_2Me, and one BCH_2CH_2 units similar to those in **7**, the spectrum shows two broad framework carbon signals which are separated by over 50 ppm (93.3 and 148.3 ppm). Contrast this to the situation for **7** (95.0 ppm for B−CH and 97.9 ppm for B−C) and other ruthenacarboranes (Table 1). Very likely the original exo-BH_2 fragment replaces the terminal hydrogen of the inserted alkyne, as shown in Scheme 3. The broad BC−*H* signal observed for similar compounds was not found for **13**, thereby corroborating this conclusion. Finally, one of the two carbonyl carbon resonances of **13** is shifted downfield (190.7 ppm) relative to those of **7** (173.5 and 176.1 ppm). This suggests coordination of the carbonyl oxygen of the $BCH_2CH_2CO_2Me$ fragment to the BH_2, similar to the interaction found in **2**. Such an intramolecular interaction is also consistent with the ^{11}B chemical shift which lies in the tetracoordinate boron range.

All attempts to grow crystals lead to slow conversion to **6** even though **13** is thermally stable. Chromatography over silica gel leads to complete decomposition of **13** to **6**. In both cases, the ultimate fates of the reduced alkyne and [BH] fragments are unknown. Clearly **7** and **13** do not lie on the reaction pathway leading to **6** in the thermally driven reaction of **1** with alkyne. Most likely hydrolytic cleavage or some closely related process leads to the cleavage of the two B−C bonds necessary to generate **6**. This observation is a significant one in the context of removing modified organic moieties from the metallaborane framework. Contrast the fate of **7** with that of its two exo BH_2 analogues generated from the reaction of **1** and MeC≡CMe or HC≡CPh. Both of these lose H_2 and yield three boron *closo* structures,[37] demonstrating that the presence of functionality on the alkyne can change the cluster reaction outcome.

A Geometric Isomer of 7 Exhibits Different Reactivity. *nido*-1,2-$(Cp^*Ru)_2(\mu$-H$)(\mu$-$BH_2)$-3-$(CH_2)_2CO_2$Me-4-CO_2Me-4,5-$C_2B_2H_4$, **14**, was isolated (4%), but attempts to grow crystals failed. The spectroscopic data establish it as a geometrical isomer of **7** (Scheme 4). Its composition based on precise mass measurement of the molecular ion yields the identical composition; the ^{11}B spectrum reveals a 3B species; the ^1H spectrum shows two Cp*, two OMe, two inequivalent B−Ht, one B−H−B, two B−H−Ru, one Ru−H−Ru hydride, the characteristic broad resonance of BC−*H* from an inserted alkyne, and two ddd hydrogen resonances for the $BCH_2CH_2CO_2Me$ unit (the $BCH_2CH_2CO_2Me$ resonances lie underneath Cp* signals as found for **13**).

The only reasonable structure for **14** is that of **7** with the orientation of the inserted alkyne reversed. This is consistent with the ∼0.7 ppm downfield shift in the BC−*H* resonance relative to **7**. Changing the location of the CCO_2Me cluster fragment relative to the $BCH_2CH_2CO_2Me$ fragment is consistent with the contrasting appearance of the methylene resonances

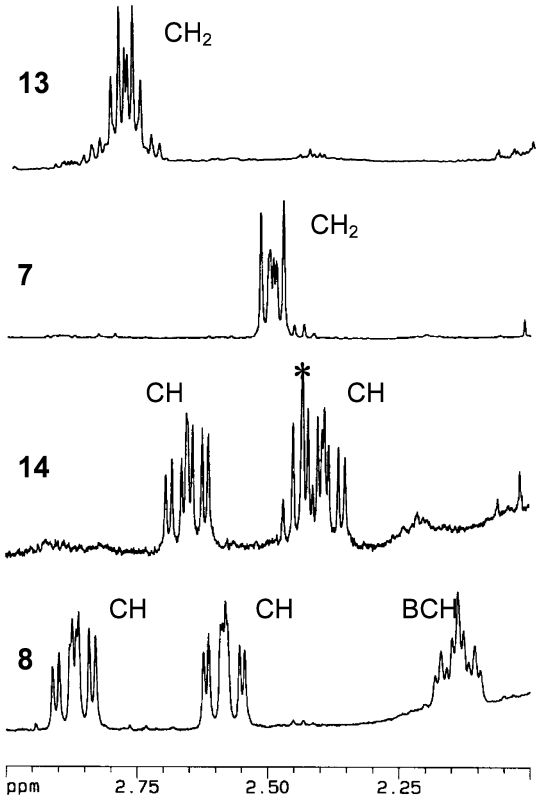

Figure 11. Comparison of the aliphatic proton resonances of the BCH_2-CH_2CO_2Me fragment in **8**, **14**, **7**, and **13**. The resonances of BCH_2CH_2 are discrete regular multiplets in **8** and **14**, but in **7** and **13** they overlap. Except for **8**, the resonances of BCH_2CH_2 are either close to or underneath Cp* signals; however, they can be observed by $^1H-^1H$ COSY (* = impurity).

of the latter. In **7**, the two proton resonances of each CH_2 are so similar in chemical shift that they appear as one single complex peak. In contrast, in **14**, the resonances of the two $BCH_2CH_2CO_2Me$ methylene protons exhibit discrete coupling patterns (Figure 11).

For **3**−**5**, the different geometrical isomers exhibit different thermal stabilities. The same is true of **7** and **14**. A 1:1 mixture of **7** and **14**, monitored by ^1H NMR at 60 °C, shows that in the time necessary to convert 20% of **7** into **13**, complete conversion of **14** to *nido*-1,2-$(Cp^*Ru)_2$-3-$(CH_2)_2CO_2Me$-4-CO_2Me-4,5-$C_2B_2H_6$, **8**, takes place. Compound **8** can also be isolated from the reaction mixture, but again attempts to grow crystals failed. Its postulated structure (Scheme 4) is based on spectroscopic data.

Precise mass measurements suggest a loss of a [BH] fragment consistent with the ^{11}B spectrum which shows two types of boron atoms in a 1:1 ratio. The ^1H spectrum reveals two Cp*, two OMe, one B−Ht, one B−CH (broad), three sets of aliphatic CH at 2.88 (ddd), 2.59 (ddd) and 2.14 (tt, broad) ppm in a ratio of 1:1:1, two B−H−Ru, and two Ru_2B triply bridging hydrogen atoms. The $^1H-^1H$ COSY spectrum (Figure 12) reveals the missing aliphatic proton resonance at 1.69 ppm under a Cp* signal. The cross-peaks show that each of the four aliphatic protons couples with the other three, consistent with the two ddd coupling patterns in the 1D proton spectrum but not the tt at 2.14 ppm. The $^1H\{^{11}B\}-^1H\{^{11}B\}$ COSY spectrum (Figure 13) provides the answer to this problem. Apart from coupling with the other three aliphatic protons, each of the BCH_2 protons is coupled to one adjacent framework proton requiring a dddd which appears as a triplet of triplets for the one unhidden

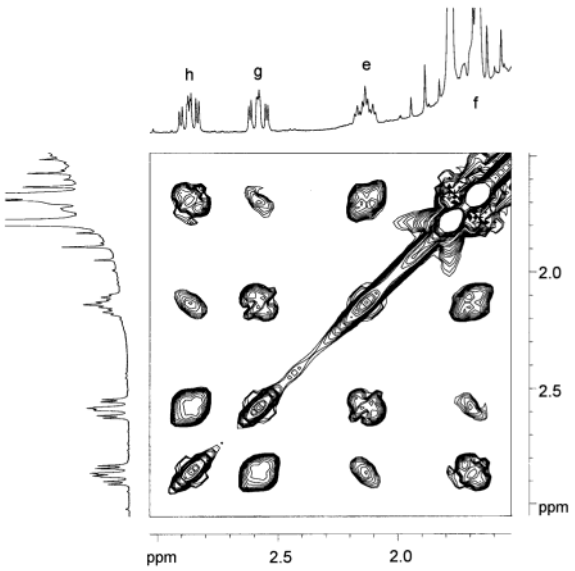

Figure 12. $^1H-^1H$ COSY spectrum in the aliphatic CH_2 region for **8** in C_6D_6. Coupling of each proton with the other three is observed.

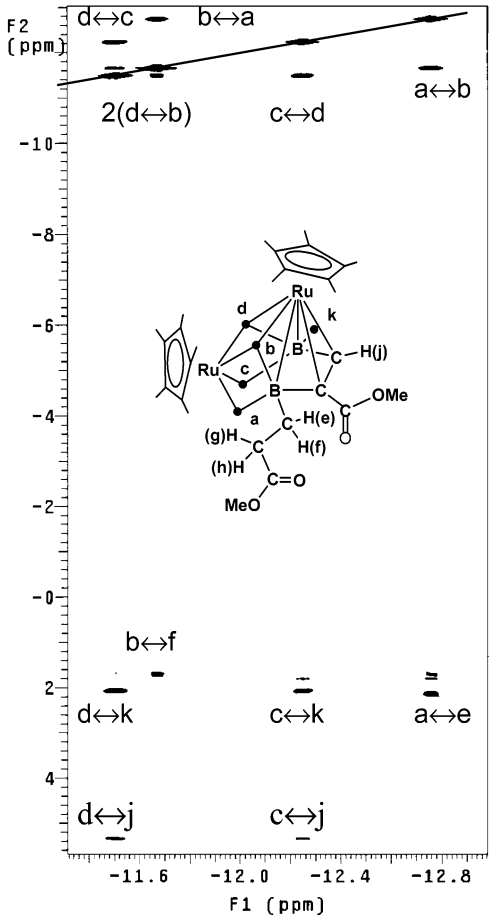

Figure 13. Partial $^1H\{^{11}B\}-^1H\{^{11}B\}$ COSY spectrum for **8** in C_6D_6 (see Supporting Information for the full spectrum). The aliphatic CH_2 protons adjacent to the cluster couple with the skeletal protons of B−H−Ru and Ru−H(B)−Ru (see the cross-peaks a ↔ e and b ↔ f). The cross-peaks between either C−H or B−Ht and the skeletal proton of either B−H−Ru or Ru−H(B)-Ru (j ↔ c and j ↔ d; k ↔ c and k ↔ d) as well as those between B−H−Ru and Ru−H(B)−Ru (a ↔ b and c ↔ d) and between the two Ru−H(B)−Ru (d ↔ b) are observed.

resonance. A 1D homonuclear decoupling experiment shows that it is the B−H−Ru proton at −12.74 ppm that couples to

Scheme 5

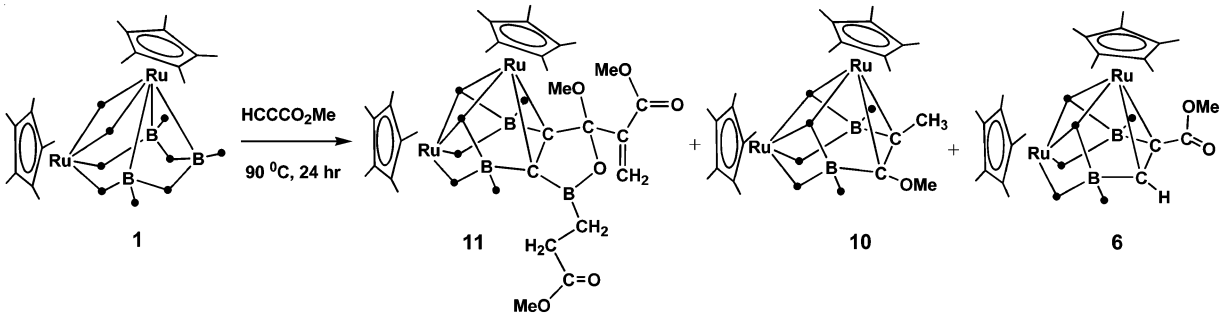

the observable BCH_2 proton (Supporting Information). Importantly, the cross-peak between the B−Ht and the C−H protons in the COSY experiment also establishes their adjacent relationship and proves that the inserted alkyne retains the orientation found in **14** (Supporting Information). The ^{13}C spectrum further confirms these conclusions.

These data indicate that the hydrocarbon fragments of **14** are retained intact and, like **7**, the reaction involves the exo-BH_2 group. Now, however, the borane is completely lost, generating the characteristic triply bridging hydrogens of a framework like that of **6**. The net effect of reversing the geometry of the inserted alkyne (**7** vs **14**) is to generate the same stable *nido*-$M_2B_2C_2$ framework, but with either BH_2 or H on the inserted alkyne carbon originating from the alkyne CH. Loss of two substituents from **13** on workup gives **6**, an unsubstituted version of **8**.

Higher Temperature Regime. Reaction **1** with an excess of methyl acetylene monocarboxylate at 90 °C for 24 h leads to a complex mixture from which **11**, **10**, and **6** are isolated as final products in yields of 37%, 5%, and 6% (Scheme 5).

The major product, *nido*-1,2-$(Cp^*Ru)_2$-4,5-B{$(CH_2)_2CO_2$-Me}CO(MeO){$C(CH_2)CO_2Me$}-4,5-$C_2B_2H_6$, **11**, is only isolated at elevated temperatures, and its complex structure is shown in Figure 14. It has the now familiar 8 sep *nido*-$Ru_2B_2C_2$ framework with the C−C edge elaborated with an organoboron fragment generated from two additional alkynes. As shown in Figure 14, the three alkynes have combined to form a planar five-membered C−C−C−O−B heterocycle. The boron atom is substituted with a hydrometalated alkyne of the type found in several kinetic products described above. The former carbonyl carbon of the inserted alkyne bears a vinyl substituent (d_{C-C} = 1.32 Å) derived from the third alkyne, and its carbonyl O atom forms part of the ring. Not only ring formation but C−C bond formation has occurred.

The spectroscopic properties of **11** confirm and add detail to the X-ray data. Of the three ^{11}B resonances observed, that assigned to the exo-cluster boron atom exhibits the downfield chemical shift expected for a three-coordinate boron atom such as that of **IV** (Scheme 1). The ^1H NMR measurements show the two terminal and four skeletal hydrogen resonances expected for the unsubstituted *nido*-$Ru_2B_2C_2$ framework. Three OMe singlets and two aliphatic CH_2 multiplets are observed (an $^1H-^1H$ COSY was required to identify the one underneath the Cp* signals) along with two doublets (J = 1.8 Hz) in the olefinic shift range. The ^{13}C spectrum confirms the $BCH_2CH_2CO_2Me$ unit and shows two sharp olefinic carbon signals plus two broad framework carbon resonances. A $^{13}C-^1H$ correlation experiment further confirms the presence of a $=CH_2$ unit through the cross-peaks between the two hydrogen resonances at 5.92 and 6.04

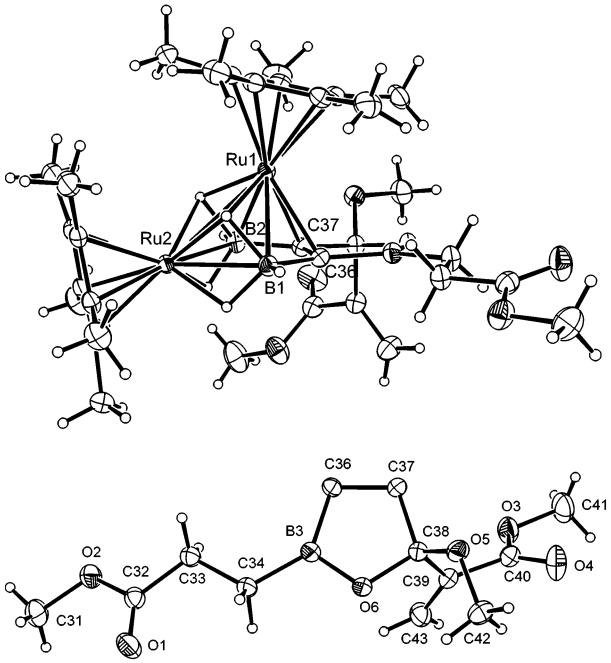

Figure 14. Molecular structure of **11**. Selected bond lengths (Å): Ru(1)−C(37) 2.1973(13), Ru(1)−C(36) 2.2032(13), Ru(1)−B(1) 2.3565(15), Ru(1)−B(2) 2.3870(16), Ru(1)−Ru(2) 2.94758(17), B(1)−C(36) 1.543(2), B(1)−Ru(2) 2.4194(15), B(2)−Ru(2) 2.3842(16), B(2)−C(37) 1.529(2), B(3)−O(6) 1.3873(19), B(3)−C(36) 1.559(2), B(3)−C(34) 1.569(2), O(5)−C(38) 1.3966(17), O(6)−C(38) 1.4375(17), C(33)−C(34) 1.520(2), C(36)−C(37) 1.4293(19), C(37)−C(38) 1.5173(19), C(38)−C(39) 1.531(2), C(39)−C(43) 1.325(2), C(39)−C(40) 1.498(2). The organoborane fragment is shown separately.

ppm and the carbon signal at 123.9 ppm. The five-membered ring requires a C−O single bond ($C_{38}-O_6$ = 1.44 Å) consistent with the upfield shift (144.4 ppm) of the corresponding ^{13}C signal. Note that one framework carbon resonance is shifted downfield ~30 ppm relative to the other. This confirms our assignment of **13** above where a similar observation was interpreted in terms of boron substitution at the framework carbon atom.

The origin of the complex alkyne condensation leading to **11** is of considerable interest. MeC≡CMe undergoes a related condensation (**IV**, Scheme 1) but with a different result. Clearly, the functional group on the alkyne is important. Given the discussion of the kinetic products presented above, a pathway to **11** is not difficult to envision. Recall **7** and its conversion to **13** (Scheme 3) and the fact that an exo-cluster bridging BH_2 fragment possesses a versatile reactivity. Thus, as shown in Scheme 6, if the exo-BH_2 of **7** reinserts into the cluster framework and extrudes the boron containing the hydrocarbyl substituent, the intermediate shown is generated. This intermedi-

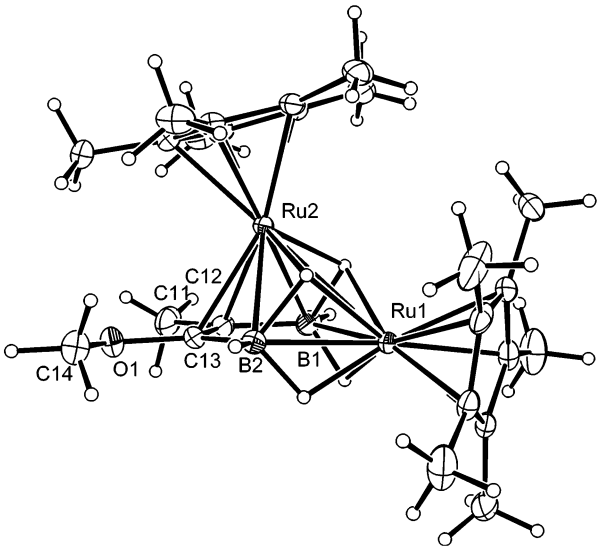

Figure 15. Molecular structure of **10**. Selected bond lengths (Å): Ru(1)−B(1) 2.381(2), Ru(1)−B(2) 2.387(2), Ru(1)−Ru(2) 2.9332(2), Ru(2)−B(1) 2.372(2), Ru(2)−B(2) 2.359(2), Ru(2)−C(12) 2.2287(19), Ru(2)−C(13) 2.2413(19), B(1)−C(12) 1.542(3), B(2)−C(13) 1.559(3), C(11)−C(12) 1.519(3), C(12)−C(13) 1.402(3), O(1)−C(13) 1.393(2), O(1)−C(14) 1.408(3).

Scheme 6

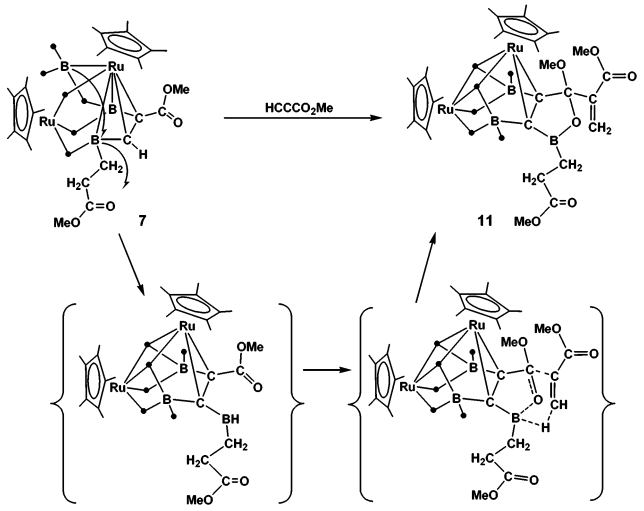

ate contains a reactive BH bond. Intramolecular coordination of the carbonyl oxygen to the boron center as found in **2** prevents B−C bond formation as observed in **IV** and also activates the carbonyl carbon for reaction. Now note from the molecular structure of **11** (Figure 14) that the $=CH_2$ group lies below the exo-cluster boron atom. If the third alkyne is oriented in the manner shown in the second intermediate, hydroboration of the triple bond concomitant with C−C bond formation at the carbonyl carbon is possible. Consistent with this hypothesis, a sample of **7** was reacted with alkyne at 90 °C. The characteristic NMR signature of **11** showed it to be a product for the reaction of **7** with alkyne.

One additional new product found under more forcing conditions is *nido*-1,2-$(Cp^*Ru)_2$-4-OMe-5-Me-4,5-$C_2B_2H_6$, **10**, and its structure (Figure 15 and confirmed by the spectroscopic data) reveals the characteristic 8 sep *nido* $Ru_2B_2C_2$ core framework. As the inserted carbon atoms bear Me and OMe substituents, **10** is most closely related to **12**. The difference is that **10** lacks the B−OH oxygen atom which was shown to arise from a carbonyl oxygen in **12**. There is also a difference in the distribution of the skeletal hydrogen atoms. An attempt to reduce **12** to **10** by using an excess of BH_3·THF at 90 °C for 24 h was not successful. As the nature of the elimination of a [BH] fragment in the conversion of **2** to **12** is unknown, it is possible that **10** is generated from an intermediate like **2** by loss of a [BOH] fragment rather than [BH]. If so, then once again it is the behavior of the "mobile" borane fragment that determines the product outcome.

Mechanistic Considerations. The overall conversion of **1** into the product mixture is considerably faster for a 1:5 reaction than for a 1:1 reaction ($t_{1/2}$ = 10 min vs 1 h). As the initial concentrations of **1** were comparable in the two reactions, this observation is consistent with the associative process expected. However, kinetic measurements were not pursued as the complexity of the reaction system considerably reduces the mechanistic value of such an analysis. This judgment is reinforced by the fact that the stoichiometry depends on reactant ratio. The number of moles of alkyne consumed per mole of **1** increases from ~1.5 to 2.5 in going from 1:1 to 1:5 ratios of **1** to alkyne. This is not particularly surprising in that the products described above demand 1, 2, and, in the case of the major product **11**, 3 mol of alkyne per mole of **1**. In an associative process, the rate of formation of each may well depend differently on the reactant ratio.

On the other hand, some of the products are formed in consecutive reactions. Further, the complete reduction or insertion of the alkyne found in the products isolated under mildest conditions suggests the existence of intermediates of lifetimes shorter than hours. We concluded it would be mechanistically most informative to seek the identity of such intermediates. Even partial characterization of species connected in time to reactants and products can significantly clarify a complex reaction path. Hence, ^1H NMR experiments were carried out to identify intermediates in the early stages of the reaction.

The presence of such intermediates was immediately confirmed as the chemical shifts of the signals observed on a time scale of minutes corresponded to none of the isolated products discussed above. At the earliest reaction time accessible by conventional NMR sampling, a set of species was observed, each of which exhibited the characteristic growth and decay of intermediates leading to some of the isolated products. Correlation of the time/intensity dependencies of the signals in the various chemical shift regions permitted assignments of some of the signals to the two earliest intermediates. Relative integrals at several different times provided a measure of the number of protons of each type for a given species. When combined with the abundant spectroscopic data for the isolated products, which were characterized by X-ray diffraction in the solid state, chemical shift comparisons permitted reasonable compositions and structures to be assigned. As will be seen, one fully defined structure is indeed mechanistically important.

Each region of the spectrum differs in the type of information most easily extracted. The methoxide region is the most informative in terms of number and abundances of species present at any given time. However, this information is of little structural value. At the other extreme, the signals associated with the reduced alkyne give the most information of mechanistic value, but the resonances are difficult to use for counting

Table 2. ^{1}H NMR Data for Intermediates **A** and **B** (the Approximate Coupling Constants, Hz, Are Shown in Parentheses)

species	MeO	Cp*	BH_T[a]	BHB[a]	RuHB	RuHRu	CH
A	3.34 s	1.55 s	3.06 br	−1.9 br t (7)	−16.2 d[a] (16)	−21.3 s	2.4 m
		1.75 s	3.09 br	−1.2 br q (6)	−10.8 br t (6)		
			4.60 br t (7)				
B	3.41 s	1.73 s	2.93 br d (7)	−4.5 br s	−11.2 t[a] (7)	−8.1 d (8)	?
		1.78 s	3.02 br	−4.6 br t (7)		−10.8 s	
			3.63 br t (6)				

[a] $\{^{11}B\}$.

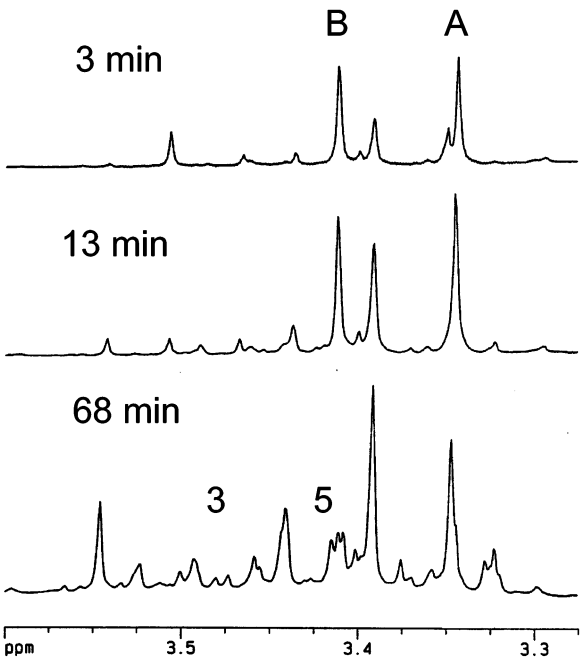

Figure 16. Proton NMR spectra of the MeO region for at 1:5 reaction mixture at short times showing the rapid formation of **A** and **B** and the much slower formation of isolated products **3** and **5**.

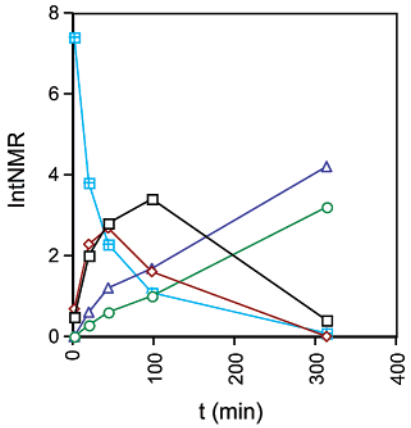

Figure 17. Relative intensities of ^{1}H MeO signals from: **A**, black; **B**, red; **3**, dark blue; **5**, green; and, for reference, the % **1** remaining × 0.05 (light blue). Note: for a 1:1 reaction with only selected species shown.

species. Our approach, which is summarized here, was to identify resonances appearing before known products, tag signals by their characteristic time dependencies, build the basic cluster framework using the NMR derived composition plus the electron counting rules, and finally address the nature of the binding of the partially reduced alkyne. This full sequence was only possible for one species, but its characterization provides clear hints on the nature of the reaction.

The methoxide region is treated first (Figure 16) at the earliest time at which there are two prominent species of approximately equal intensity (**A**, **B**). Somewhat later, a third grows to comparable intensity, and then at ∼1 h five species are prominent (the chemical shift of one is very close to that of **A**). At about the same time, the first signs of compounds **3**, **5** are seen and **A** and **B** pass through their maximum intensities. Signals in other spectral regions are observed that can be attributed to the three later intermediates; however, these data were insufficient in number to define either the composition or the alkyne−ruthenaborane interaction and are not discussed further. For **A** and **B**, the data given in Table 2 for the characteristic regions of the spectrum analyzed below provided nearly complete assignments. Thus, in these two cases, there was sufficient information to generate a reasonable composition. The time dependences of the abundances of **1**, **3**, **5**, **A**, and **B** are shown in Figure 17, where it may be seen that those of **A** and **B** describe the classic behavior of intermediates lying between **1** and **3**, **5**.

The Cp* region is consistent with the data from the MeO region and shows that both **A** and **B** have inequivalent Cp*Ru fragments. Relative to **1**, the perturbation of the metal fragments is larger for **B** than **A**. Two B−H−B and three BH_t resonances were observed for both **A** and **B**, suggesting the presence of a (BH)−H−(BH)−H−(BH) fragment as found in **1**, albeit the perturbation of this fragment in **A** is now larger than that in **B**. Taken together, these data suggest the framework connectivity of **1** is largely retained and that the alkyne perturbs the borane fragment of **A** more than that of **B** and the metal fragment of **B** more than that of **A**. The $^1H\{^{11}B\}$ B−H−B resonances of **A** are multiplets, and the quartet observed for one shows the presence of a B(H)−H−B(H)−H−Ru fragment which in turn suggests an unusual endohydrogen distribution like that of **2**. Taken with the triplet observed for the other B−H−B resonance, the connectivity $B(H)-H_{trip}-B(H)-H_{quart}-B(H)-H_{trip}-Ru$ is established. Compound **B**, however, exhibits a different coupling pattern in the B−H−B resonances that is more suggestive of a $B-H_{trip}-B(H_{trip})-H_{trip}-Ru$ fragment. The other B−H−B resonance appears to be of a type similar to that found in **5**. As the principal kinetic products, **3**−**5**, preserve the basic framework composition of **1**, the data already point to a process similar to that in Scheme 2 in which *arachno* **2** is an intermediate in the formation of *nido* **12**.

The hydride region is the next most complex one and adds structural detail to the framework. Based both on intensity/time dependence and on ^{1}H decoupling data, a Ru−H−Ru proton and a Ru−H−B proton can be easily associated with **A**. Importantly, as shown below, the latter is a doublet. Clearly associated with **B** are a Ru−H−Ru proton (doublet) and a Ru−H−B proton (triplet). In addition, in the coupled spectrum there is a sharp signal superimposed on a broad signal at δ −10.8

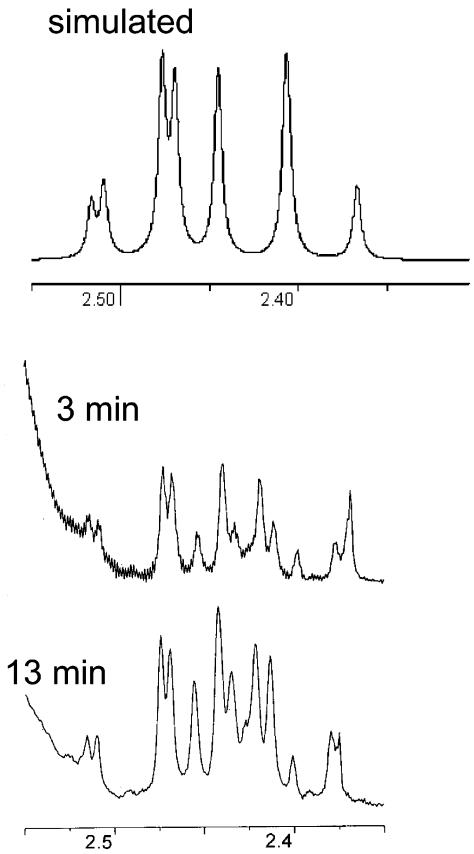

Figure 18. Bottom: observed ^{1}H signals in the CH region for a 1:5 reaction at two early reaction times. Top: simulated ^{1}H spectra in the CH region. Note: the doublet (dd calc'd) at δ −16.2 associated with this multiplet is not shown.

Chart 1. Schematic Representation of Intermediate **A** and Comparison with the Known Structures of **2** and **5**

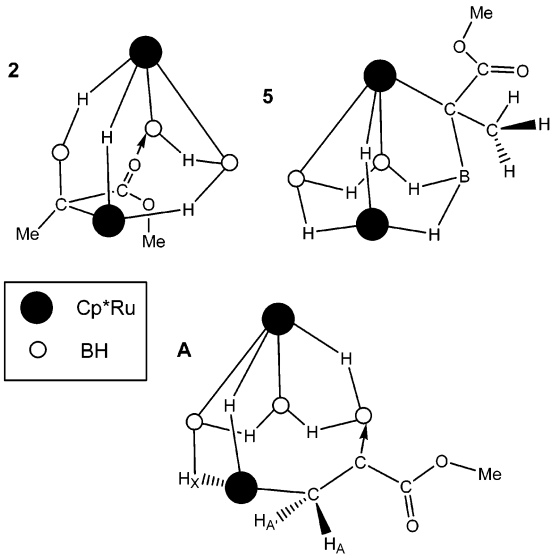

that appears to be associated with **A** or **B**. The time dependence of the sharp signal appears more characteristic of **B** than **A**. In the decoupled spectrum, the broad signal becomes a partially hidden triplet slightly downfield of the singlet. These multiplicities are consistent with the discussion of the BHB resonances above. No other hydride signals with intensity/time profiles consistent with **A** or **B** are evident. Hence, **B** possesses two Ru−H−Ru (the low chemical shifts are also consistent with terminal hydrides) and one Ru−H−B, whereas the opposite is the case for **A**; that is, as compared to **1**, **A** is missing a Ru−H−Ru and **B** is missing a Ru−H−B hydrogen. In terms of the ruthenaborane fragment alone, these products both contain odd electron $Cp^*_2Ru_2H_3(B_3H_5)$ moieties. Hence, the hydrocarbyl fragment derived from the alkyne must contribute an odd number of electrons to cluster bonding; more than simple coordination is necessary. Possibly **A** and **B** are isomers differing in only the site of alkyne addition.

One CH region is shown in Figure 18 for two reaction times immediately after placing the sample in the NMR probe. The shift region is characteristic of methylene protons in compounds such as, for example, **7**. Variations of intensity with time show that the multiplet contains contributions from at least two species. The intensity change with time illustrated in Figure 18 allows the assignment of five signals to a species with highest abundance at earliest times. These signals constitute a second-order multiplet which requires binding of a CH_2 fragment in a site that generates magnetically inequivalent protons. A satisfactory simulation of the observed resonances was obtained for an AA′X system (CHH′−RuH″) and is shown in Figure 18. Two cases were investigated. In both, the X proton was taken to be a framework hydride (Ru−H−B for **A** and Ru−H−Ru for **B**) and the hydride chemical shift δ (H_X) and one CH−RuH coupling constant for **A** and **B** (J_{HX-HA}) were fixed at the observed values (Table 2). Reasonable agreement of peak positions and intensities was obtained using four variables: δ (H_A, $H_{A'}$) = 2.41, 2.49, $J_{HA-HA'}$ = 16.0 Hz, and the second $J_{HX-HA'}$ = 2 Hz for **A**. No good fit to the observed multiplet could be generated for **B**. The intensity/time dependence of the underlying multiplet suggests it is not associated with **B**, but we were unable to unambiguously identify any other CH signals associated with **B**.

The postulated structure of intermediate **A** is shown in Chart 1. Because of the similarity and magnitudes of the chemical shifts as well as the magnitude of the $H_A-H_{A'}$ coupling constant, a CH_2 fragment is indicated rather than a CH−CH fragment. The preferential coupling of the metal hydride to one of the CH_2 protons suggests both a three-bond coupling constant and a favorable dihedral angle for one but not the other proton, that is, a bridged structure with direct bonding to at least one metal atom. It is possible that in **A** hydroruthenation leads to a CH_2 group sigma bound to the basal ruthenium atom, thereby generating coupling of the methylene proton to the framework hydride which resides in a favorable geometrical relationship. Compound **8**, discussed above, is a precedent. A carbene center is necessarily generated, and its coordination to the most accessible basal B atom leads to the bridged structure shown. The bridge generates selective coupling to the metal hydride. Coordination of the carbon lone pair leads to cluster opening and the *arachno* structure shown. An analogous cluster opening involving intramolecular carbonyl oxygen coordination to a boron site was found in **2** described above and serves as precedent. The proposed structure of **A** is also satisfying in terms of subsequent product formation. Transfer of another H to the carbon atom of the CH_2 group leads directly to a methyl carboxylate fragment directed away from the RuHRu edge. Simultaneous closure of the Ru apical B basal edge generates the observed *nido* product **5**.

Although **A** is only one of several intermediates observed, its identification and structural characterization are significant. Considering the rich variation in structure and reactivity resulting from the various isomeric forms of isolatable compounds, for example, **3**−**5** and **7**, **14**, it is likely that intermediate **B** and the others present are variations on **A**. The initial step appears to be hydrometalation which leads to formation of the Ru−B bridged alkylidene products **3** and **5** or the hydrocarbyl substituted boron atom. Insertion appears to follow a different route, and the one already described to account for the chemistry in Scheme 1[37] likely operates in parallel with the hydrometalation route described here. The latter requires a terminal alkyne. Both pathways require simultaneous interaction with ruthenium and boron sites. This synergistic effect resulting from the combination of metal and boron in a single cluster species shows that metallaboranes are more than simple structural analogues of metal clusters and borane cages. This work, as well as earlier studies of less complex metallaboranes,[53−57] show that metallaboranes are species with considerable chemical potential for the manipulation of organic substrates.

Experimental Section

General Procedures. All operations were conducted under argon atmosphere using standard Schlenk techniques.[58] Solvents were dried with appropriate reagents and distilled before use under N_2. $LiBH_4$ (2 M in THF), HC≡CCO_2Me (Aldrich), and [(Cp*$RuCl_2$)n] (Strem) were used as received. *nido*-1,2-(Cp*Ru)$_2B_3H_9$ was prepared according to the literature procedures.[4] Silica gel (ICN 32−63, 60 Å) was purchased from ICN Biomedicals GmbH and predried at 180 °C before use. NMR spectra were recorded on a Bruker AMX 400 or a Varian 500 FT-NMR spectrometer. Residual proton signals of solvents were used as reference: ^{1}H (δ, ppm, benzene-d_6, 7.16); and ^{13}C (δ, ppm, benzene-d_6, 128.39; acetone-d_6, 29.92 and 206.68). For ^{11}B an external reference was used: a sealed capillary containing [(Me_4N)(B_3H_8)] in acetone-d_6 (δ, ppm, −29.7). Infrared spectra were measured on a Perkin-Elmer Paragon 1000 FT-IR spectrometer. Mass spectra were obtained on a JEOL LMS-AX505 spectrometer using the EI or FAB ionization modes.

Synthesis of 2, 3, 4, 5, 6, 14, 7, 8, 16. To an orange solution of **1** (150 mg, 0.29 mmol) in hexane (30 mL) was added HC≡CCO_2Me (0.32 mL, 3.6 mmol). The resulting solution was stirred for 8 h at ambient temperature during which the color changed into orange-red. After removal of solvent and excess of alkyne, the residue was chromatographed. Elution with hexane/toluene (2:1) gave **2** (23 mg, 13%); further elution gave **3** (17 mg, 10%) with hexane/ether (20:1); **4** (7 mg, 4%) and **5** (17 mg, 10%) with hexane/ether (10:1); **6** (27 mg, 16%) with hexane/ether (5:1); **14** (7.9 mg, 4%), **7** (17.8 mg, 9%), **8** (15.6 mg, 8%), and **16** (12.7 mg, 7%) with hexane/ether (1:2).

2. ^{1}H{^{11}B} (C_6D_6): δ 5.49 (d, J = 10 Hz, 1H, B−Ht), 4.95 (s, 1H, B−Ht), 3.94 (d, J = 10 Hz, 1H, B−Ht), 3.14 (s, 3H, OMe), 1.95 (s, 3H, CH_3), 1.87 (s, 15H, Cp*), 1.75 (s, 15H, Cp*), −1.34 (q, J = 10 Hz, 1H, B−H−B), −12.39 (s, 1H, Ru−H−Ru), −13.18 (d, J = 10 Hz, 1H, B−H−Ru), −18.02 (s, br 1H, B−H−Ru). ^{11}B (C_6D_6): δ 27.7, 18.6, 15.5 (1:1:1). ^{13}C (C_6D_6): δ 10.97 (Cp*), 12.07 (Cp*), 24.25 (CH_3), 54.52 (OMe), 88.79 (Cp*), 94.41 (Cp*), 182.69 (CO). IR (KBr): ν 2429 (B−H), 1502, 1455 (COO). MS (70 ev): m/z (%) M^+ (90). Calcd, 600.1616 for $C_{24}H_{43}B_3O_2Ru_2$; found, 600.1640.

3. ^{1}H{^{11}B} (C_6D_6): δ 3.64 (t, J = 5.0 Hz, 2H, B−Ht), 3.48 (s, 3H, OMe), 1.89 (s, 15H, Cp*), 1.78 (s, 15H, Cp*), 1.45 (s, 3H, CH_3), −2.62 and −2.63 (partially overlapping, 2H, B−H−B), −11.14 (s, 1H, B−H−Ru), −11.41 (t, J = 5.0 Hz, 1H, B−H−Ru), −14.56 (s, 1H, Ru−H−Ru). ^{11}B (C_6D_6): δ 19.6, 19.0, 8.8 (1:1:1). ^{13}C (C_6D_6): δ 10.47 (Cp*), 12.51 (Cp*), 22.62 (CH_3), 50.47 (OMe), 58.85 (br C−B), 88.18 (Cp*), 96.06 (Cp*), 178.38 (CO). IR (KBr): ν 2498, 2448 (B−H), 1690 (COO). MS (70 ev): m/z (%) M^+ (95). Calcd, 600.1628 for $C_{24}H_{43}B_3O_2Ru_2$; found, 600.1653.

4. ^{1}H{^{11}B} (C_6D_6): δ 3.73 (br 1H, B−Ht), 3.44 (br 1H, B−Ht), 3.42 (s, 3H, OMe), 2.79 (d, br J = 14 Hz, 1H, CH), 2.66 (dd, J_1 = 4.4 Hz, J_2 = 14 Hz, 1H, CH), 2.24 (dd, J_1 = 14 Hz, J_2 = 14 Hz, 1H, CH), 1.82 (s, 15H, Cp*), 1.74 (s, 15H, Cp*), −2.38 (t, J = 5.0 Hz, 1H, B−H−B), −3.47 (t, J = 5.0 Hz, 1H, B−H−B), −10.63 (t, J = 5.0 Hz, 1H, B−H−Ru), −11.35 (s, 1H, B−H−Ru), −15.40 (s, 1H, Ru−H−Ru). ^{11}B (C_6D_6): δ 19.7, 11.8, 10.7 (1:1:1). ^{13}C (C_6D_6): δ 10.59 (Cp*), 12.61 (Cp*), 43.53 (CH_2), 51.19 (OMe), 57.36 (br C−B), 86.35 (Cp*), 95.34 (Cp*), 174.78 CO). IR (KBr): ν 2493, 2438 (B−H), 1725 (COO). MS (FAB): m/z (%) [M^+ − H] (100). Calcd, 599.1551 for $C_{24}H_{42}B_3O_2Ru_2$; found, 599.1545.

5. ^{1}H{^{11}B} (C_6D_6): δ 4.02 (t, J = 5.0 Hz, 1H, B−Ht), 3.42 (s, 3H, OMe), 3.41 (partially overlapping with OMe, 1H, B−Ht), 1.76 (s, 15H, Cp*), 1.73 (s, 15H, Cp*), 1.59 (s, 3H, CH_3), −1.71 (t, J = 5.0 Hz, br 1H, B−H−B), −2.22 (t, J = 5.0 Hz, 1H, B−H−B), −11.49 (t, J = 5.0 Hz, 1H, B−H−Ru), −11.66 (s, 1H, B−H−Ru), −15.33 (s, 1H, Ru−H−Ru). ^{11}B (C_6D_6): δ 18.1, 17.3, 11.8 (1:1:1). ^{13}C (C_6D_6): δ 9.93 (Cp*), 12.48 (Cp*), 26.69 (CH_3), 50.23 (OMe), 56.37 (br C−B), 87.21 (Cp*), 96.14 (Cp*), 179.36 (CO). IR (KBr): ν 2557, 2525, 2461 (B−H), 1663 (COO). MS (FAB): m/z (%) [M^+ − 4H] (100). Calcd, 596.1316 for $C_{24}H_{39}B_3O_2Ru_2$; found, 596.1308.

6. ^{1}H{^{11}B} (C_6D_6): δ 5.53 (s, br 1H, CH), 3.58 (s, 3H, OMe), 2.72 (t, J = 7.0 Hz, 1H, B−Ht), 2.22 (t, J = 7.0 Hz, 1H, B−Ht), 1.78 (s, 15H, Cp*), 1.74 (s, 15H, Cp*), −11.59 (t, J = 7.0 Hz, 1H, Ru−H−Ru), −11.69 (t, J = 7.0 Hz, 1H, Ru−H−Ru), −12.25 (t, J = 7.0 Hz, 1H, Ru−H−B), −12.42 (t, J = 7.0 Hz, 1H, Ru−H−B). ^{11}B (acetone-d_6): δ −14.2, −15.2 (1:1). ^{13}C (acetone-d_6): δ 10.77 (Cp*), 12.12 (Cp*), 50.84 (OMe), 88.80 (Cp*), 93.41 (Cp*), 96.58 (br C=***C***H), 175.42 (CO). IR (KBr): ν 2468 (B−H), 1604, 1373, and 1222 (COO). MS (70 ev): m/z (%) M^+ (100). Calcd, 586.1297 for $C_{24}H_{40}B_2O_2Ru_2$; found, 586.1290.

14. ^{1}H{^{11}B} (C_6D_6): δ 5.36 (s, br 1H, C−H), 4.44 (br 1H, B−Ht), 4.25 (br 1H, B−Ht), 3.50 (s, 3H, OMe), 3.42 (s, 3H, OMe), 2.65 (ddd, J_1 = 5.0 Hz, J_2 = 12.2 Hz, J_3 = 13.8 Hz, 1H, CH_2), 2.39 (ddd, J_1 = 5.0 Hz, J_2 = 12.2 Hz, J_3 = 13.8 Hz, 1H, CH_2), 1.83 (s, 15H, Cp*), 1.56 (s, 15H, Cp*), −2.46 (s, 1H, B−H−B), −11.19 (s, 1H, B−H−Ru), −14.91 (s, 1H, B−H−Ru), −15.69 (s, 1H, Ru−H−Ru). ^{11}B (C_6D_6): δ 28.4, 23.4, 20.9 (1:1:1). MS (FAB): m/z (%) M^+ (7). Calcd, 684.1840 for $C_{28}H_{47}B_3O_4Ru_2$; found, 684.1827.

7. ^{1}H{^{11}B} (C_6D_6): δ 4.68 (s, br 1H, C−H), 4.47 (br 1H, B−Ht), 3.68 (br 1H, B−Ht), 3.52 (s, 3H, OMe), 3.46 (s, 3H, OMe), 2.51 (m, 2H, CH_2), 1.70 (s, 15H, Cp*), 1.53 (s, 15H, Cp*), 1.32 (m, 2H, CH_2), −2.33 (s, 1H, B−H−B), −10.94 (s, 1H, B−H−Ru), −14.99 (s, 1H, Ru−H−Ru), −15.10 (s, 1H, B−H−Ru). ^{11}B (C_6D_6): δ 28.0, 26.3, 12.0 (1:1:1). ^{13}C (C_6D_6): δ 10.07 (Cp*), 11.78 (Cp*), 21.63 (br B−CH_2), 34.51 (CH_2), 50.90 (OMe), 51.30 (OMe), 89.67 (Cp*), 94.79 (Cp*), 95.02 (br H−***C***−B), 97.88 (br C−B), 173.52 (CO), 176.11 (CO). IR (KBr): ν 2490, 2442 (B−H), 1734, 1696 (COO). MS (FAB): m/z (%) [M^+−H] (70). Calcd, 683.1762 for $C_{28}H_{46}B_3O_4Ru_2$; found, 683.1797.

8. ^{1}H{^{11}B} (C_6D_6): δ 5.34 (s, br 1H, C−H), 3.54 (s, 3H, OMe), 3.46 (s, 3H, OMe), 2.88 (ddd, J_1 = 4.9 Hz, J_2 = 12.8 Hz, J_3 = 15.3 Hz, 1H, CH), 2.59 (ddd, J_1 = 4.3 Hz, J_2 = 12.8 Hz, J_3 = 15.3 Hz, 1H, CH), 2.14 (dddd, J_1 = J_2 = 4.3 Hz, J_3 = J_4 =12.8 Hz, 1H, CH), 2.08 (br 1H, B−Ht), 1.79 (s, 15H, Cp*), 1.69 (dddd, J_1 = J_2 = 4.9 Hz, J_3 = J_4 =12.8 Hz, 1H, CH), 1.67 (s, 15H, Cp*), −11.49 (t, J = 6.0 Hz, 1H, Ru−H(B)-Ru), −11.66 (d, J = 6.0 Hz, 1H, Ru−H(B)-Ru), −12.24 (br 1H, B−H−Ru), −12.74 (t, J = 6.0 Hz, 1H, B−H−Ru). ^{11}B

(53) Burgess, K.; Ohlmeyer, M. J. *Chem. Rev.* **1991**, *91*, 1179.
(54) Chen, H.; Schlecht, S.; Semple, T. C.; Hartwig, J. F. *Science* **2000**, *287*, 1995.
(55) Iverson, C. N.; Smith, M. R., III. *J. Am. Chem. Soc.* **1999**, *121*, 7696.
(56) Pender, M. J.; Carroll, P. J.; Sneddon, L. G. *J. Am. Chem. Soc.* **2001**, *123*, 12222.
(57) Kawano, Y.; Yasue, T.; Shimoi, M. *J. Am. Chem. Soc.* **1999**, *121*, 11744.
(58) Shriver, D. F.; Drezdzon, M. A. *The Manipulation of Air-Sensitive Compounds*, 2nd ed.; Wiley-Interscience: New York, 1986.

Table 3. Crystallographic Data and Structure Refinement Information for **3**, **4**, **5**, **2**, **12**

	3	**4**	**5**	**2**	**12**
formula	$C_{24}H_{43}B_3O_2Ru_2$	$C_{24}H_{43}B_3O_2Ru_2$	$C_{24}H_{43}B_3O_2Ru_2$	$C_{24}H_{43}B_3O_2Ru_2$	$C_{24}H_{42}B_2O_2Ru_2$
formula weight	598.15	598.15	598.15	598.15	586.34
cystal system	triclinic	triclinic	orthorhombic	monoclinic	monoclinic
space group	*P*-1	*P*-1	*Pbca*	*P*2(1)/*c*	*P*2(1)/*n*
a (Å)	8.7820 (3)	8.6927 (5)	8.8737 (5)	11.4297 (7)	8.5080 (4)
b (Å)	15.8777 (6)	12.2929 (7)	17.6413 (9)	14.8019 (9)	13.9030 (6)
c (Å)	19.9676 (8)	12.4232 (7)	33.5339 (18)	15.4447 (9)	21.8889 (9)
α (deg)	71.2020 (10)	97.8350 (10)	90	90	90
β (deg)	80.1060 (10)	93.9480 (10)	90	93.0530 (10)	92.2130 (10)
γ (deg)	88.8040 (10)	102.1810 (10)	90	90	90
V (Å^3)	2594.75 (17)	1278.97 (13)	5249.5 (5)	2609.2 (3)	2587.2 (2)
Z	4	2	8	4	4
D_{calc} (g/cm^3)	1.531	1.553	1.514	1.523	1.505
F(000)	1224	612	2448	1224	1200
μ (mm^{-1})	1.182	1.199	1.169	1.175	1.184
crystal size (mm)	0.3 × 0.1 × 0.02	0.3 × 0.2 × 0.2	0.4 × 0.4 × 0.4	0.3 × 0.2 × 0.04	0.4 × 0.15 × 0.15
θ range (deg)	2.00−30.52	2.20−30.49	2.31−25.00	1.91−30.52	1.86−30.52
min, max trans	1.0000, 0.8984		1.0000, 0.9230	1.0000, 0.8046	1.0000, 0.8745
no. reflns. collected	32 631	16 076	40 786	31 460	31 864
no. unique reflns. (R_{int})	15 773 (0.0185)	7780 (0.0150)	4628 (0.0280)	7964 (0.0589)	7886 (0.0275)
data/restraints/ parameters	15 773/0/657	7780/0/293	4628/0/323	7964/0/287	7886/0/331
GOF	1.032	1.034	1.103	1.001	1.056
R indices ($I > 2\sigma(I)$)	$R_1 = 0.0254$	$R_1 = 0.0215$	$R_1 = 0.0304$	$R_1 = 0.0337$	$R_1 = 0.0268$
	$wR_2 = 0.0606$	$wR_2 = 0.0542$	$wR_2 = 0.0751$	$wR_2 = 0.0804$	$wR_2 = 0.0642$
R indices (all data)	$R_1 = 0.0289$	$R_1 = 0.0234$	$R_1 = 0.0311$	$R_1 = 0.0449$	$R_1 = 0.0304$
	$wR_2 = 0.0624$	$wR_2 = 0.0553$	$wR_2 = 0.0756$	$wR_2 = 0.0840$	$wR_2 = 0.0660$
largest diff. peak and hole (e/Å^3)	1.083, −0.341	1.159, −0.583	2.286, −0.832	1.342, −0.996	1.319, −0.439

(C_6D_6): *δ* −1.4, −15.3 (1:1). ^{13}C (C_6D_6): *δ* 10.81 (Cp*), 12.14 (Cp*), 17.82 (br B−CH_2), 35.49 (CH_2), 50.63 (OMe), 51.14 (OMe), 88.46 (Cp*), 92.73 (Cp*), 93.86 (br C−B), 97.53 (br H−C−B), 175.20 (CO), 176.77 (CO). IR (KBr): *ν* 2442 (B−H), 1735, 1696 (COO). MS (FAB): *m*/*z* (%) M^+ (100). Calcd, 672.1669 for $C_{28}H_{46}B_2O_4Ru_2$; found, 672.1687.

16. ^{1}H{^{11}B} (C_6D_6): *δ* 3.44 (s, 3H, OMe), 2.82 (br 1H, B−Ht), 2.37 (br 1H, B−Ht), 1.73 (s, 15H, Cp*), 1.68 (s, 15H, Cp*), 0.45 (br 2H, B−OH), −11.56 (t, *J* = 6.5 Hz, 1H, Ru−H(B)−Ru), −11.58 (t, *J* = 6.5 Hz, 1H, Ru−H(B)−Ru), −12.51 (br 1H, B−H−Ru), −12.67 (t, *J* = 6.5 Hz, 1H, B−H−Ru). ^{11}B (C_6D_6): *δ* 31.8, −8.8, −11.1 (1:1:1). IR (KBr): *ν* 3244 (O−H), 2477, 2401 (B−H). MS (70 ev): *m*/*z* (%) M^+ (20). Calcd, 630.1371 for $C_{24}H_{41}B_3O_{4\delta}Ru_2$; found, 630.1335.

Synthesis of 10 and 11. To an orange solution of **1** (150 mg, 0.29 mmol) in toluene (20 mL) was added HC≡CCO_2Me (0.32 mL, 3.6 mmol). The resulting solution was stirred for 24 h at 90 °C, during which the color of the mixture changed into dark-red. After removal of solvent and an excess of alkyne, the residue was chromatographed. Elution with hexane/toluene (1:2) gave **10** (8.3 mg, 5%), and further elution with hexane/ether (5: 1) gave **6** (10 mg, 6%) and **11** (82.4 mg, 37%). Heating **7** (25 mg, 0.036 mmol) and HC≡CC(O)Me (0.32 mL, 3.6 mmol) in toluene (15 mL) for 24 h at 90 °C under argon leads to **11** and **6** based on ^{1}H and ^{11}B NMR spectra of the reaction mixture.

10. ^{1}H{^{11}B} (C_6D_6): *δ* 3.61 (s, 3H, OMe), 2.18 (s, 3H, CH_3), 2.03 (t, *J* = 7.0 Hz, 2H, B−Ht), 1.85 (s, 15H, Cp*), 1.83 (s, 15H, Cp*), −10.92 (t, *J* = 7.0 Hz, 1H, Ru−H(B)−Ru), −11.52 (t, *J* = 7.0 Hz, 1H, Ru−H(B)−Ru), −12.44 (t, *J* = 7.0 Hz, 1H, B−H−Ru), −12.63 (t, *J* = 7.0 Hz, 1H, B−H−Ru). ^{11}B (C_6D_6): *δ* −17.1, −23.6 (1:1). ^{13}C (C_6D_6): *δ* 11.42 (Cp*), 12.32 (Cp*), 18.99 (CH_3), 58.61 (OMe), 86.33 (Cp*), 91.04 (Cp*). IR (KBr): *ν* 2456, 2428 (B−H). MS (70 ev): *m*/*z* (%). EI: [M^+ − H] (30). Calcd, 571.1430 for $C_{24}H_{41}B_2ORu_2$; found, 571.1426.

11. ^{1}H{^{11}B} (C_6D_6): *δ* 6.04 (d, *J* = 1.8 Hz, 1H, CH), 5.92 (d, *J* = 1.8 Hz, 1H, CH), 3.45 (s, 3H, OMe), 3.40 (s, 3H, OMe), 3.33 (s, 3H, OMe), 2.87 (m, 2H, CH_2), 2.23 (br 1H, B−Ht), 2.10 (br 1H, B−Ht), 1.84 (s, 15H, Cp*), 1.80 (m, 2H, CH_2), 1.75 (s, 15H, Cp*), −11.79 (t, *J* = 7.0 Hz, 1H, Ru−H(B)−Ru), −11.83 (t, *J* = 7.0 Hz, 1H, Ru−H(B)−Ru), −12.23 (t, *J* = 7.0 Hz, 1H, B−H−Ru), −12.90 (t, *J* = 7.0 Hz, 1H, B−H−Ru). ^{11}B (C_6D_6): *δ* 52.4, −15.0, −18.7 (1:1:1). ^{13}C (C_6D_6): *δ* 11.98 (Cp*), 12.34 (Cp*), 14.10 (br B−CH_2), 30.14 (CH_2), 51.29 (OMe), 51.31 (OMe), 51.99 (OMe), 87.45 (Cp*), 92.52 (Cp*), 101.06 (br C−B), 113.66 (***C***═CH_2), 123.95 (C═***C***H_2), 133.99 (br C−B), 144.35 (CO), 167.12 (CO), 175.68 (CO). IR (KBr): *ν* 2435 (B−H), 1738 (COO). MS (FAB): *m*/*z* (%) [M^+ − 2H] (40). Calcd, 766.1895 for $C_{32}H_{49}B_3O_6Ru_2$; found, 766.1887.

Synthesis of 12. Compound **2** (36 mg, 0.06 mmol) in a NMR tube (C_6D_6, 0.7 mL) was heated for 48 h at 80 °C under argon to lead to complete conversion to **12**. Chromatography by elution with hexane/ether (1:2) gave **12** (29 mg, 82%). ^{1}H{^{11}B} (C_6D_6): *δ* 3.57 (s, 3H, OMe), 2.33 (br, s, 1H, BOH), 2.10 (s, 3H, CH_3), 1.85 (s, 30H, Cp*), 1.58 (br 1H, B−Ht), −11.21 (d, *J* = 12.0 Hz, 1H, B−H−Ru), −12.15 (d, *J* = 5.0 Hz, 1H, B−H−Ru), −12.33 (s, 1H, Ru−H−Ru), −13.11 (s, 1H, B−H−Ru). ^{11}B (C_6D_6): *δ* 16.3, −24.7 (1: 1). ^{13}C (C_6D_6): *δ* 11.15 (Cp*), 12.38 (Cp*), 18.81 (CH_3), 59.07 (OMe), 87.65 (Cp*), 91.82 (Cp*), 95.46 (br C−B), 100.28 (br C−B). IR (KBr): *ν* 3588 (O−H), 2412 (B−H). MS (70 ev): *m*/*z* (%) M^+ (20). Calcd, 588.1445 for $C_{24}H_{42}B_2O_2Ru_2$; found, 588.1491.

Synthesis of 13. Compound **7 (**26 mg, 0.038 mmol) in a NMR tube (C_6D_6, 0.7 mL) was heated for 30 min at 80 °C under argon to lead to complete conversion to **13**. Chromatography by elution with hexane/ether (5: 1) gave **6** (19 mg, 87%). **13**. ^{1}H{^{11}B} (C_6D_6): *δ* 3.93 (t, *J* = 6.0 Hz, 1H, B−Ht), 3.38 (s, 3H, OMe), 3.32 (s, 3H, OMe), 2.78 (m, 2H, CH_2), 2.24 (br 1H, B−Ht), 1.77 (s, 15H, Cp*), 1.71 (s, 15H, Cp*), 1.57 (m, 2H, CH_2), −11.52 (t, *J* = 6.0 Hz, 1H, Ru−H(B)−Ru), −11.67 (t, *J* = 6.0 Hz, 1H, Ru−H(B)−Ru), −11.79 (br 1H, B−H−Ru), −12.65 (br 1H, B−H−Ru). ^{11}B (C_6D_6): *δ* 11.82, −14.74, −17.81 (1:1:1). ^{13}C-(C_6D_6): *δ* 10.79 (Cp*), 12.30 (Cp*), 20.72 (br B−CH_2), 33.60 (CH_2), 50.85 (OMe), 55.68 (OMe), 87.69 (Cp*), 91.46 (Cp*), 93.32 (br C−B), 148.30 (br B−C−B), 177.15 (CO), 190.68 (CO). MS (FAB): *m*/*z* (%) [M^+ − 3H] (20). Calcd, 681.1606 for $C_{28}H_{44}B_3O_4Ru_2$; found, 681.1639.

Proton NMR at Early Reaction Times. The reaction of **1** with methyl acetylene monocarboxylate was monitored in a 1:1 and 1:5 ratio,

Table 4. Crystallographic Data and Structure Refinement Information for **6**, **16**, **7**, **11**, **10**

	6	**16**	**7**	**11**	**10**
formula	$C_{24}H_{40}B_2O_2Ru_2$	$C_{24}H_{41}B_3O_4Ru_2$	$C_{28}H_{47}B_3O_4Ru_2$	$C_{32}H_{51}B_3O_6Ru_2$	$C_{24}H_{42}B_2ORu_2$
formula weight	584.32	628.14	682.23	766.30	570.34
cystal system	orthorhombic	triclinic	triclinic	triclinic	monoclinic
space group	*Pbca*	*P*-1	*P*-1	*P*-1	*P*2(1)/*n*
a (Å)	15.592 (3)	10.9258 (7)	8.5760 (4)	8.7990 (4)	8.3722 (4)
b (Å)	15.598 (3)	16.0455 (11)	10.5548 (5)	13.0672 (6)	19.8606 (8)
c (Å)	20.518 (4)	16.0955 (11)	18.5784 (9)	15.6891 (7)	15.1043 (6)
α (deg)	90	89.7750 (10)	73.6990 (10)	101.3620 (10)	90
β (deg)	90	88.8930 (10)	83.9850 (10)	100.4420 (10)	95.6380 (10)
γ (deg)	90	74.1490 (10)	66.9360 (10)	101.2970 (10)	90
V (Å^3)	4990.1 (18)	2713.9 (3)	1485.03 (12)	1688.34 (13)	2499.35 (19)
Z	8	4	2	2	4
D_{calc} (g/cm^3)	1.556	1.537	1.526	1.507	1.516
F(000)	2384	1280	700	788	1168
μ (mm^{-1})	1.228	1.140	1.048	0.935	1.221
crystal size (mm)	0.34 × 0.17 × 0.08	0.25 × 0.22 × 0.06	0.2 × 0.2 × 0.1	0.4 × 0.3 × 0.3	0.4 × 0.3 × 0.2
θ range (deg)	1.99−25.00	1.94−25.06	2.17−30.54	2.37−30.50	2.05−30.53
min, max trans	0.8015, 0.5428	1.0000, 0.8429	1.0000, 0.9174	1.0000, 0.9211	1.0000, 0.9051
no. reflns. collected	38 587	22 352	18 663	21 286	30 819
no. unique reflns. (R_{int})	4400 (0.0772)	9581 (0.0439)	9017 (0.0225)	10 245 (0.0158)	7617 (0.0186)
data/restraints/ parameters	4400/0/271	9581/0/595	9017/0/385	10 245/0/439	7617/0/304
GOF	1.432	1.029	1.068	1.064	1.162
R indices ($I > 2\sigma(I)$)	$R_1 = 0.0699$	$R_1 = 0.0427$	$R_1 = 0.0441$	$R_1 = 0.0231$	$R_1 = 0.0269$
	$wR_2 = 0.1303$	$wR_2 = 0.0949$	$wR_2 = 0.0959$	$wR_2 = 0.0591$	$wR_2 = 0.0644$
R indices (all data)	$R_1 = 0.0765$	$R_1 = 0.0644$	$R_1 = 0.0518$	$R_1 = 0.0250$	$R_1 = 0.0278$
	$wR_2 = 0.1323$	$wR_2 = 0.1035$	$wR_2 = 0.0999$	$wR_2 = 0.0602$	$wR_2 = 0.0649$
largest diff. peak and hole (e/Å^3)	0.938, −1.577	1.648, −0.691	1.552, −1.640	0.781, −0.432	1.680, −0.926

respectively, in a NMR tube in C_6D_6 under argon at ambient temperature. The spectra were recorded on a Bruker AMX 400 spectrometer using a spectral width of 20 000 Hz and a relaxation delay of 3 s between pulses. The residual proton signal of the solvent was used as reference (δ, 7.16 ppm).

X-ray Crystallography. Crystals suitable for X-ray analysis were obtained by slow evaporation of the hexane solution at ambient temperature, except **16** in ether/hexane and **7** in pentane at −40 °C. Crystal data were collected on a Bruker Apex system with graphite monochromated Mo Kα (λ = 0.71073 Å) radiation at 100 K. The structure was solved by direct methods and refined using SHELXL-97 (Sheldrick, G. M., University of Göttingen). Non-hydrogen atoms were found by successive full matrix least squares refinement on F^2 and refined with anisotropic thermal parameters. Hydrogen atom positions were placed at idealized positions except for B−H and Ru−H, which were located from difference Fourier maps. A riding model was used for subsequent refinements of the hydrogen atoms, with fixed thermal parameters [$u_{ij} = 1.2U_{ij}$(eq) for the atom to which they are bonded], again except for B−H and Ru−H, in which case the thermal parameters were allowed to refine independently. Crystallographic information for compounds **2**−**7**, **10**−**12**, and **16** is given in Tables 3 and 4.

Acknowledgment. This work was supported by the National Science Foundation CHE 9986880.

Supporting Information Available: The selective proton homonuclear decoupled spectrum and the full $^1H\{^{11}B\}-^1H\{^{11}B\}$ COSY spectrum of **8** (PDF), and X-ray crystallographic files (CIF) for compounds not previously communicated: **4**, **7**, **10**, **11**, **16**. This material is available free of charge via the Internet at http://pubs.acs.org.

JA038444T